MICHIGAN STATE UNIVERSITY

CYCLOTRON LABORATORY

DAMPING OF NUCLEAR EXCITATIONS

G. F. BERTSCH, P. F. BORTIGNON and R. A. BROLIA

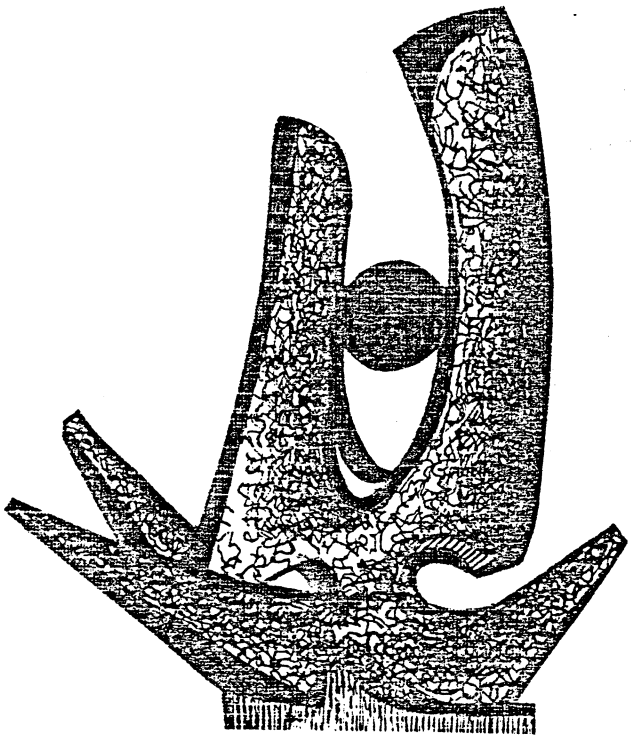

AUGUST 1982

MSUCL-381

DAMPING OF NUCLEAR EXCITATIONS

G.F. Bertsch

National Superconducting Cyclotron Laboratory
and Department of Physics
Michigan State University
East Lansing, Michigan 48824

and

P.F. Bortignon

University of Padova, Istituto di Fisica Galileo Galilei,
Padova; and INFN, L.N. Legnaro, Italy

and

R.A. Broglia

The Niels Bohr Institute
University of Copenhagen
DK-2100 Copenhagen Ø, Denmark

To be published in "Reviews of Modern Physics" January, 1983 issue

TABLE OF CONTENTS

Abstract

We review the theory and the empirical evidences of damping of simple nuclear excitations, namely particle states and vibrational states. The particle damping phenomena include the optical model description of elastic scattering, fragmentation of single-particle levels, and systematics of neutron strength functions. Information on the known collective vibrational states is summarized and compared with theory.

A theoretical model that has found considerable success is based on a damping mechanism in which the simple excitations mix with the surface vibrations. This implies that the surface damping dominates for excitation energies below about 15 MeV. There is a close relation between the single-particle damping and the damping of collective vibrations. However, the vibrational damping is strongly suppressed by the coherence between the particle and the hole. While the model reproduces many of the observed features of the data rather well, it tends to underpredict the spreading width by as much as a factor of two. Thus other degrees of freedom, not well understood at present, may play a role in the damping.

I. INTRODUCTION

A goal of nuclear structure theory is an understanding of the damping of simple nuclear excitations such as single-particle states and collective vibrations. The subject is an old one, beginning with Bohr's picture of the nucleus as a highly overdamped system, the compound nucleus (Bohr, 1936). Later, elastic neutron scattering experiments showed that single-particle motion could persist across the diameter of the nucleus, and this led to the first quantitative description of damping, the optical model. By now we have a thorough knowledge of the single-particle motion, not only from elastic scattering but also from spectroscopic studies with transfer reactions, and to some extent from inelastic scattering reactions. The study of nuclear vibrations also has an early beginning, dating from the discovery of the giant dipole resonance in the photoabsorption cross section. In recent years inelastic scattering experiments have unveiled a rich variety of vibrations of different types. All these vibrational modes are characterized by the quantum numbers of orbital angular momentum, spin angular momentum, and isospin. The vibrations are observed as peaks in the energy distribution of inelastic scattering, peaks from which the mean energy, the strength, and the damping width are extracted.

The properties of a nuclear excitation can be most conveniently discussed in terms of its strength function, defined as

$$S(E) = \sum_i \langle i|\mathcal{O}|o\rangle^2 \delta(E - E_i) \qquad (1)$$

Here $\langle i|\mathcal{O}|o\rangle$ is the matrix element of the operator creating the mode. The operator is evaluated between the initial state o and the eigenstates i of the nucleus. The function S(E) contains far more than is needed to describe the damping of the mode; for example, it contains the individual eigenenergies of the states. Averaging S over an energy interval preserves the gross features of the strength function while discarding the fine details. If the averaged S is a peaked function having a width substantially larger than the energy averaging interval, one can speak of the (mean) energy of the mode and its width Γ. The experimental strength functions are generally already averaged to the extent that only the gross features are visible. For the theoretical strength function, the averaging is an essential formal device to introduce damping.

The theory of the strength function in the absence of coupling to more complex degrees of freedom is now well understood in terms of mean field theory. The single-particle motion is described by a static Hartree-Fock Hamiltonian. With just a few parameters to characterize the Hamiltonian, the varied shell structure of nuclei across the periodic table can be explained. Treating the single-particle potential as a dynamic quantity, the vibrations of the nucleus around the ground state can be calculated with surprising accuracy. This is the RPA theory of the vibrations. It provides a good description both of the mean energies of the various modes, and of the detailed structure of the low-lying vibrational states.

At all but the lowest excitation energies, the simple modes are embedded in a complex spectrum and mix with the nearby states.

The purpose of this review is to assess our present understanding of this mixing, which requires a level of theory beyond the mean field approximation. One approach of course is to try to calculate the entire spectrum using the shell model as a basis. This is impractical in most cases. It is also unnecessary for determining the gross features of the strength function. We only need to compute the mixing of the simple modes with excitations at the next level of complexity. These states, called doorways, may in turn mix with still more complicated states, but this mixing should not affect the averaged properties of the strength function for the simple modes. The width of a state due to mixing with more complex configurations we denote by $\Gamma^{\downarrow}$, to be distinguished from the escape width $\Gamma^{\uparrow}$, which is associated with the decay by particle emission.

Our review begins with a summary of the experimental information on single-particle and vibrational damping. We then discuss the theory, treating the damping of particle excitations and of vibrations in turn. Our theoretical review will emphasize the appropriate description of the doorway states, using the knowledge gained from the mean field theory of the simple modes. At low excitation energies the only important degrees of freedom are the surface vibrations, and the simple modes will decay by exciting them. At higher energies, the nucleons in the interior of the nucleus absorb energy more effectively from the simple modes. Obviously, there are close connections between the damping of different kinds of modes. Vibrations can be viewed as particle-hole

states, so the same mechanisms that damp the particle excitations will operate for vibrations. However, the quantitative relationship is somewhat subtle, because the coherence which gives the particle-hole state its vibrational character also affects the damping. As we shall see, the coherence reduces the coupling to other degrees of freedom, and thereby decreases the damping. It is for this reason that vibrational excitations can be seen as peaks in the strength functions at much higher energy than single particle states can be identified.

On a numerical level, the calculated widths are generally within a factor of two of the empirical values. However, there is a systematic tendency for the empirical damping to be underestimated by theory, showing that our understanding is not yet complete. The theoretical strength function often has much more structure than experiment. The doorways themselves must be strongly mixed with states of even higher complexity. A complete description of damping would require an understanding of the mixing at each level of complexity, but this remains for the future.

II. EMPIRICAL SINGLE-PARTICLE DAMPING

There are several ways to get information on the single-particle properties of nuclei. States near the Fermi surface can be studied by transfer reactions, such as (^{3}He,d) for measuring the particle strength function, or (^{3}He,α) for measuring the hole strength function. Well above the Fermi surface the particle states are unbound and then can be studied by the direct scattering of nucleons. Since the nucleon-nucleus interaction is well described by the optical model, the information about the propagation of the nucleon in the nucleus can be summarized in the optical model parameters. Information about the deeply bound hole states is more difficult to obtain, with the most reliable data coming from the (e,e'p) knockout reaction. We will now examine in detail the information obtained about damping by these different methods.

A. Spectroscopic study of single-particle fragmentation

When the single-particle strength is studied by transfer reactions, the orbital angular momentum of the transferred particle can be determined from the angular distribution of the reaction. The experimental angular distribution is compared with predictions for different ℓ-transfers based on the Distorted Wave Born Approximation (DWBA). Comparison of the absolute magnitude of the cross section allows one to infer the matrix element of the particle creation or annihilation operator between the initial and final nuclear states. The square of this matrix element is known as the spectroscopic strength. The normalization is such that the maximum spectroscopic strength for a shell of angular momentum j is equal to the number of possible particles in the shell, $2j+1$.

There are two points of caution to be kept in mind in using the DWBA analysis. First, without polarization data it is only possible to measure the orbital angular momentum of the transferred particle. The j must be inferred from other considerations. Second, the DWBA is an uncontrolled approximation and there is an uncertainty in the overall normalization of the spectroscopic strengths. Because of the correlations between nucleons, part of the single-particle strength is shifted to very high energies, and one should not expect to see all of the theoretical strength in these spectroscopic experiments.

A classic example illustrating the spectroscopic application of tranfer reactions is the $^{48}Ca(^3He,d)^{49}Sc$ reaction, which populates proton states in the double magic ^{48}Ca target. The orbits populated will be those just above the Fermi surface, which are $f_{7/2}$, $p_{3/2}$ and $p_{1/2}$. In Fig. 1 is shown the strengths for the different angular momentum transfer seen in this reaction (Erskine, et al., 1966). The $f_{7/2}$ ground state has a spectroscopic factor close to 8, the maximum for this orbital, and is thus essentially a pure configuration. The p-wave strength lies at an excitation of about 5 MeV, and it mixes with other states. The $p_{3/2}$ is split into at least two major parts. The $p_{1/2}$ lies higher in energy and is divided over several states. In the case of the next higher orbital, the $f_{5/2}$ orbital, no single state has more than 25% of the total strength.

At higher excitation energies the level density becomes too large and individual states cannot be resolved in the transfer reactions. It is still possible to study the single-particle excitations by the envelope of the strength distribution, which appear as a broad bump in a low-resolution experiment. Again, the angular

distribution of this bump is used to assign the ℓ-transfer. This analysis has been mainly used to study orbits deeply bound below the Fermi surface. An example in the study of proton orbits is the reaction $^{90}Zr(\vec{d},^3He)^{89}Y$, measured by Stuirbrink, et al., (1980). The energy spectrum of the ^3He at a scattering angle of 11 degrees is shown in Fig. 2. We see a prominent bump, shown shaded in the figure, which is identified as $f_{7/2}$ from the angular distribution and polarization data. Unfortunately, there is a substantial background under the bump, which must be subtracted out before the analysis can be made. There is as yet no good theory for the background, causing some additional errors. The inferred mean energy of the $f_{7/2}$ strength is 6.8 MeV, and the width is 4 MeV. The extracted spectroscopic strength for the whole bump is 10. Since 8 is the theoretical maximum, this gives some indication of the uncertainties in the theoretical analysis of the data.

An example of a neutron transfer process is provided by the reaction $^{116}Sn(d,t)^{115}Sn$, used to study the high-ℓ orbits in ^{115}Sn (Siemssen, et al., 1981). A spectrum is shown in Fig. 3. The broad bump in the spectrum has an angular distribution characteristic of high angular momentum. The areas marked I - IV are assigned to $g_{9/2}$, $p_{1/2}$ and $p_{3/2}$ and the area V is assigned to $f_{5/2}$, $p_{1/2}$ and $p_{3/2}$ orbits. The total spectroscopic strength of the $g_{9/2}$ is found to be 11.3 ± 2, close to the expected value 9 for a filled $j = 9/2$ shell. The quantity of main interest to us is the width, which is about 3-4 MeV. It is difficult to make this more precise because there is an intermediate structure of

peaks within the main bump. The $f_{5/2}$ strength is much smoother, lying at higher excitation energy, and the width is determined to be 8 MeV. A similar reaction was used to study the $h_{11/2}$ hole strength in ^{207}Pb (Gales, et al., 1978). As is found for the $g_{9/2}$ in Sn, the experimental spectrum shows a broad bump with superimposed sharper peaks. The width was determined to be 3.8 MeV. However, only half the total strength was found within the bump. Since the missing strength is probably part of the higher energy background, the assigned width should be considered a lower limit.

In Table I we compile the information on particle widths obtained from transfer reactions. To summarize the data, widths are of the order of 4 MeV for excitation energies between 5 and 10 MeV, and are considerably larger at higher excitation energies. As we shall see later, the theory of infinite Fermi systems predicts that the width should increase as the square of the energy for low excitation energies,

$$\Gamma^{\downarrow} = aE^2 \qquad (2)$$

Here E is the excitation energy of the nucleon measured from the Fermi energy. From the transfer reaction data in Table I, we infer a value for the proportionality constant

$$a \approx \frac{1}{15\ \text{MeV}} - \frac{1}{20\ \text{MeV}} \qquad (3)$$

The parameterization

$$\Gamma^{\downarrow} = (24\ \text{MeV})\ \frac{E^2}{E_0^2 + E^2} \qquad (4)$$

was used by Brown and Rho (1981) to fit the energy dependence of the single-particle width in medium light nuclei (cf. Mahaux and Ngo, 1981). In eq. (4), the constant E_0^2 is 500 MeV^2. For particles near the Fermi energy ($E \lesssim 10$ MeV) this is equivalent to eq. (2) with

$$a = \frac{1}{20\ \text{MeV}}$$

At the higher excitation energies, the particle transfer reaction is not as suitable as other methods to single-particle widths. Our primary information about the very deeply bound hole states is from the (e,e'p) reaction, reviewed some time ago (Jacob and Maris, 1973). The most deeply bound orbit, the $1s_{1/2}$, can be seen in nuclei up to ^{40}Ca. From the ^{40}Ca(e,e'p)^{39}K reaction, the excitation energy of the $0s_{1/2}$ hole is found to be about 50 MeV and its width is about 30 MeV (Nakamura, et al., 1974; Mougey, et al., 1976).

B. Single-particle states in the continuum

1. The neutron strength function

The strength of low-ℓ orbits near the neutron threshold can be studied by the properties of the resonances in the neutron scattering reaction $n + A \rightarrow (A+1)^*$. The level density of the $(A+1)^*$ nucleus is generally high, but the low energy of the scattering neutron, going down to thermal energies, makes it possible to resolve individual levels. The average width of the levels, $\langle \Gamma_i/D \rangle$, is proportional to the single particle strength. The constant of proportionality depends on the velocity of the scattering neutron; this dependence is factored out in the usual definition of the strength function

$$S_\ell = \left\langle \frac{\Gamma_i}{D} \left(\frac{1eV}{E_i}\right)^{\ell+\frac{1}{2}} \right\rangle \qquad (5)$$

Here D is the average distance between resonances, and E_i is the neutron incident energy. The strength functions for s- and p-waves show a well-known resonance behavior, when plotted as a function of mass A. This may be seen in the plots of S_0 and S_1 in Figs. 4 and 5, from Mughabghab and Garber, (1973). The s-wave strength peaks near masses A = 50 and A = 150, indicating that an s-orbit is near zero binding for these nuclei, and that the damping is insufficient to obliterate the shell structure. The p-wave strength peaks at masses between the s-wave maxima, as expected for the zero-binding states of a particle in a potential well.

The optical model provides a theoretical framework for describing the strength function (Feshbach, Porter, and Weisskopf, 1954). The scattering states of a particle are computed for a

potential well that has an imaginary part. The asymptotic form of the optical wave function has the form

$$U_\ell(r) = e^{ikr} + \eta_\ell e^{-ikr} e^{-2i\delta_\ell}$$

where the reflection coefficient η is a real number between zero and one. The connection between the strength function and the optical wave function is

$$\eta = 1 - \pi \left\langle \frac{\Gamma}{D} \right\rangle \qquad (6)$$

The curves in Figs. 4 and 5 are obtained from eq. (6) with the following optical potential,

$$U(r) = -V_0 f(x) + i4W_D \frac{df(x)}{dx} \qquad (7)$$

where

$$f(x) = (1 + \exp((r - r_0 A^{1/3})/a_0))^{-1}$$

$r_0 = 1.35$ fm $\quad a_0 = 0.65$ fm $\quad V_0 = 41.5 - 43.5$ MeV $\quad W_D = 5.4$ MeV

The effect of the imaginary potential is to smear out the single-particle strength function, broadening the peaks and filling in the minima. From the figures, the width in A of the strength function peak is about 1/5 of the spacing between peaks. Correspondingly, the optical potential should give a width in energy of about 1/5 of the energy spacing of the s-wave single-particle states, i.e. about 4 MeV. More quantitatively, we may evaluate the expectation of the imaginary optical potential, eq. (7), for a weakly bound s-wave orbital, using eq. (28). This yields a width of about 4 MeV, which is included in the compilation of Table I.

2. The optical model in elastic scattering

At higher energies, information about the single-particle propagation is obtained from the angular distributions in elastic scattering. In principle the elastic scattering can be analyzed partial wave by partial wave, to study each angular momentum state separately, but in practice one uses the optical model to fit the entire angular distribution. An example of the partial wave behavior is found in a study of the elastic scattering reaction $^{16}O(p,p)^{16}O$ (Skwiersky, Baglin and Parker, 1974). The extracted phase shift and reflection coefficient of the $f_{7/2}$ partial wave is shown in Fig. 6. These scattering parameters were determined from optical model fits to the data at each energy. As the energy of the proton increases, the phase shift rises through 90°. At the same time the absorption in the f wave increases, with the reflection coefficient dropping from 0.8 to 0.2 over the interval studied. The increasing absorption of the $f_{7/2}$ partial wave over the energy region is mainly due to the increased penetration of the wave at higher energy; the strength of the imaginary potential has only a modest increase over the energy interval.

The systematic behavior of the optical potential can best be seen by a global fit of the optical parameters to a large body of data. An example of this kind of analysis is the global potential for neutron scattering below 30 MeV, made by Rapaport, et al. (1979). Their absorptive potential is surface-peaked below 15 MeV neutron scattering energy. The absorption increases with energy in this region, and these authors assume a linear form for the energy dependence.

Above 15 MeV neutron energy, the absorption changes smoothly to a volume form. The specific parameterization of their potential is

$$iW(r) = 4iW_D \frac{df}{dx} - iW_V f(x) \qquad (8)$$

$$\text{with } r_0 = 1.295 \text{ fm}, \; a = 0.59 \text{ fm}$$

$$\left.\begin{aligned} W_D &= 4.28 + 0.4E - \frac{N-Z}{A}\, 12.8 \text{ MeV} \\ W_V &= 0 \end{aligned}\right\} \; E < 15 \text{ MeV}$$

$$\left.\begin{aligned} W_D &= 14.0 - 0.39E - 10.4\, \frac{N-Z}{A} \text{ MeV} \\ W_V &= -4.3 + 0.38E \end{aligned}\right\} \; E > 15 \text{ MeV}$$

where E is the neutron scattering energy. The sudden onset of the volume potential at 15 MeV is obviously an artifact of the parameterization; clearly there is some ambiguity in determining the radial dependence of the absorption.

The volume integral of the optical potential provides a measure of its strength that is insensitive to the radial parameterization of the potential (Agrawal and Sood, 1975). For the higher scattering energies, between 20 MeV and 200 MeV, the volume integral of the absorptive potential is roughly independent of energy. Also, it is roughly proportional to the atomic mass of the nucleus, and has a magnitude

$$J_W = \frac{1}{A} \int d^3r \; W(r) \cong 100 \pm 10 \text{ MeV-fm}^3 \qquad (9)$$

For lower energies, the volume integral is more dependent on the nuclear mass. For example, the volume integral of the neutron resonance potential, eq. (7), varies from $J_W = 80$ MeV-fm^3/n at mass 60 to $J_W = 50$ MeV-fm^3/n at mass 108.

It is instructive to relate the spreading widths of single particle states to the absorptive volume integral, eq. (9). The spreading width from eq. (28) is given by

$$\Gamma = 2 \int \rho_i W \, d^3r \sim 2\bar{\rho}_i \int W \, d^3r \qquad (10)$$

where $\bar{\rho}_i$ is an average density of the single-particle orbitals in the vicinity of the absorptive region. As a rough estimate, we can take the average density for a particle in the absorptive potential region to be half nuclear matter density,

$$\bar{\rho}_i \sim 0.08 \text{ fm}^{-3}/A \qquad (11)$$

Using the volume integral of eq. (9) this yields a spreading width

$$\Gamma^{\downarrow} \sim 2(100A \text{ MeV-fm}^3) \frac{0.08 \text{ fm}^{-3}}{A} \sim 16 \text{ MeV} \qquad (12)$$

This is quite a large spreading, of the order of the shell spacing, showing that no shell structure should be expected at higher excitation energies. The spreading width of the 0s hole state in Table I is quite a bit larger than the estimate (12) from the optical potential for particles. This is by no means a contradiction; the damping depends on the momentum of the orbital as well as its excitation energy. A deeply bound orbital has low momentum, and is therefore expected to interact more strongly with other bound nucleons. However, further study is called for in the interpretation of the (e,e'p) experiment, particularly the role of the final state proton in spectral widths.

III. EMPIRICAL DAMPING OF VIBRATIONS

Many kinds of nuclear vibration have now been identified. For recent reviews, see (Bertrand, 1980; Speth and van der Woude, 1981). In this section, we will merely summarize the experimental situation, referring the reader to these reviews for a more complete picture with the primary references to the experimental data. Typically, the response to an external field shows a resonant peak in some region of excitation energy. The character of the external field determines the kind of vibration excited. The field can have a dependence on the spin and isospin of the nucleons, as well as a spatial dependence that resolves into multipoles. The peaks of the giant vibrations are embedded in a spectrum of very high level density, and the spreading of the response can be directly measured by the width of the experimental strength distributions.

An important theoretical tool for interpreting strength distributions is the energy-weighted sum rule. A sum rule may be defined for each multipolarity, following (Bethe and Levinger, 1950) and (Satchler, 1972). A peak in the strength function may be considered a giant vibration if its strength exhausts most of the sum rule.

A. The giant dipole vibration

The earliest and best known example of a nuclear vibration is the giant dipole resonance. This is a vibration of neutrons against protons, and is excited by the long-wavelength isovector dipole field, $V(r) \sim \tau_z \vec{r}$. It exhausts about 100% of the sum rule calculated without exchange corrections. The systematic behavior of the dipole vibration was last reviewed by Berman and Fultz (1975). It is visible in nuclei as light as ^{4}He, as may be seen from the

photoneutron cross section in Fig. 7. Here the peak is quite broad, due to the escape of particles into the continuum. In heavy nuclei, the escape width is relatively small, and the damping is mainly due to mixing with more complicated states. The empirical evidence for this is based on the decay properties of the excitation. The dipole state in heavy nuclei decays primarily by emitting low energy neutrons, just like the more complex states in the same region of excitation. If the escape width were important, a large portion of the decays would emit energetic particles, populating the simple configurations of the daughter nucleus. Experimentally, only about 15% of the decays are of this type, showing that the escape width is of the order of 15% of the total width (Kuchnir, et al., 1967). Fig. 8 shows a typical dipole response in a heavy spherical nucleus ^{208}Pb. The shape is well fit by the Lorentzian function,

$$S(E) = \frac{2S_0}{\pi} \frac{E^2\Gamma}{(E^2-E_0'^2)^2 + E^2\Gamma^2} \qquad (13)$$

with resonance energy $E_0' = 14$ MeV and width $\Gamma = 4$ MeV. In eq. (13). S_0 is the integrated strength, and $E_0'^2 = E_0^2 + (\Gamma/2)^2$, where E_0 is the energy of the dipole mode in the absence of the couplings responsible for the width Γ.

The systematics of the dipole width as a function of mass is shown in Fig. 9. Note that the width is particularly small near magic nuclei. This shows the importance to the damping of the low-energy degrees of freedom, which fluctuate in strength from nucleus

to nucleus, and are particularly weak in magic nuclei. Deformed nuclei show a double-peaked structure in the dipole response (Fig. 10). The frequency of the dipole vibration depends on the size of the nucleus along the dipole axis, and it follows that there are two different frequencies in an axially deformed nucleus. This coupling of the dipole to the quadrupole shape degree of freedom suggests a damping mechanism. We shall see later how this is exploited in the adiabatic model of damping.

B. Density vibrations: quadrupole, monopole and octupole

We now turn to the isoscalar vibrations, in which the neutrons and protons move in phase. The most thoroughly studied giant vibration of this kind is the giant quadrupole. This vibration is excited by inelastic scattering of electrons and various nuclear projectiles. Alpha particles have been particularly useful, since to a good approximation they only excite the isoscalar modes, for energies $\lesssim$200 MeV (cf. eg. Buenerd, 1981). The giant quadrupole vibration is seen in all nuclei from ^{16}O to ^{238}U. Most of the quadrupole strength can be resolved into individual states in the alpha scattering reaction on light nuclei such as ^{24}Mg (Bertrand, et al., 1978). The experimental integrated strength distribution of ^{24}Mg(α,α')^{24}Mg is shown in Fig. 12, compared to the Breit-Wigner distribution, assuming a width $\Gamma^{\downarrow} = 8$ MeV.

The total observed strength is found to be nearly 100% of the sum rule, when the usual procedure is followed on normalizing the projectile-target interaction to fit the elastic scattering. A typical spectrum showing the giant quadrupole bump in heavy nuclei is shown in Fig. 11, for the reaction ^{90}Zr(α,α')^{90}Zr at 152 MeV bombarding energy. There is a clear peak standing on a uniform background. However, there will be some uncertainty in the extracted strength associated with the shape assumptions about the background and the peak shape. The systematics of the quadrupole widths as a function of nuclear mass is plotted in Fig. 13. In light nuclei the state is rather broad, of the order of 8 MeV wide. For ^{16}O, there is an important direct decay component by α-particle emission (Knöpfle, et al., 1978). Thus the large total width in light nuclei may be partly due to $\Gamma^{\uparrow}$, the escape width. In heavy nuclei the

escape width becomes small, as in the case of the dipole vibration. Nevertheless it has been possible to observe a direct decay branch in a heavy system, ^{119}Sn (Okada, et al., 1982).

One topic of recent interest in the damping of the giant quadrupole vibration is the fission decay in very heavy nuclei (Ströher, et al., 1982, and refs. therein). Naively, if the damping into complex configurations were very weak, one might expect an enhanced fission branch because the quadrupole motion carries the nucleus toward a fissioning shape. Experimentally, the fission decay is not enhanced over background; there is some controversy about whether it is suppressed with a recent experiment by Dowell, et al., (1982) showing no suppression. Theoretically, it would be astonishing if the giant quadrupole vibration had a fission decay any different from the background states. We see that the state decays very quickly into more complex nuclear excitations, being spread over several MeV. It requires a much longer time for the nucleus to fission or finally decay by neturon emission. All memory of the entrance channel should have been lost by this time.

There is one important difference between results of electron scattering and alpha-particle scattering that is not understood. According to the analysis of alpha scattering reactions, about 70% of the quadrupole sum rule is contained in the giant vibration. A similar result was also found from inelastic proton scattering at 200 MeV (Djalali, et al., 1982). However, the electron scattering data indicates a lower value, 50% of less (Kühner, et al., 1981). Obviously, this needs to be resolved before the theory can be assessed on a really quantitative level.

Giant vibrations have also been observed in the isoscalar response for $L = 0$ and $L = 3$ multipoles. The $L = 0$ mode, the giant monopole vibration, is best excited by small angle scattering of strongly absorbed projectiles. It is located in energy just above the quadrupole vibration, and appears in most spectra as a shoulder on the quadrupole peak. Fig. 14 shows an example of the angular distribution of alpha particles, exhibiting the forward

peak characteristic of $L = 0$ transfer (Youngblood, et al., 1977). The vibration is only visible in nuclei larger than ^{40}Ca, and has a width of about 3 MeV in the heavier nuclei. Recently, the giant octupole vibration has been identified in heavy spherical nuclei. It is considerably higher in energy than the other vibrations discussed, having a mean energy in the range of 18-20 MeV for ^{208}Pb. The inelastic background scattering at these excitation energies makes it difficult to accurately determine the energy width of the vibration as well as its total strength. However, different experiments agree on a width of the order of 5 MeV in ^{208}Pb (Carey, et al., 1980), (Morsch, et al., 1980), (Yamagata, 1982). In lighter nuclei, the width is somewhat larger, ranging up to 10 MeV in ^{40}Ca.

C. Spin vibrations

There has been great progress recently in the study of spin vibrations, due to the availability of a reaction which is quite specific for this mode. In the previously described modes, the nucleon spins were not affected by the excitation process, and consequently the excitations carry spin $S = 0$. In principle, there are two kinds of spin excitation possible, isoscalar and isovector, depending on whether the coupling to protons and neutrons is the same or not. The (p,n) reaction at 100-200 MeV bombarding energy, which of course has isovector character, has been found to be quite specific to excite spin vibrations. The simplest such excitation is created by the operator $\sigma\tau_-$ with no spatial dependence. This is just the Gamow-Teller beta decay operator. Since there is no momentum transfer, the angular distribution in the inelastic

scattering will be forward peaked. Some typical spectra at 0° are shown in Fig. 15, from (Gaarde, et al., 1981). Of the nuclei having a neutron excess, the Gamow-Teller peak is a rather prominent feature of the spectrum. Nuclei with N = Z do not have the Gamow-Teller state because the spins are almost all paired in the ground state wave function. The width of the Gamow-Teller state is about 4 MeV, and its excitation energy in the residual nucleus varies from about 10 MeV in lighter nuclei to 15 MeV in ^{209}Pb.

The (p,n) reactions at nonzero scattering angles excite modes with orbital angular momentum as well as spin. The $(Y_L\sigma)_J\tau_-$ response with L = 1 is found to have a peak somewhat higher in energy than Gamow-Teller state, but with a much larger width, about 10 MeV in ^{208}Pb (Horen, et al., 1980). This is much larger than the widths we have so far encountered for states of moderate excitation energy. However, not all of the width is due to spreading into more complex configurations or particle decay. The orbital and spin angular momentum can couple three different total angular momenta J, and the strength functions are expected to peak at different energies (Bertsch, et al., 1981). Unfortunately, to distinguish the different total angular momenta in the strength function would require difficult spin polarization measurements.

Another spin excitation operator, which is close to the electromagnetic M1 transition operator, is σt_z. In principle the M1 strength can be excited by electron scattering or by the (p,p') reaction. However, this vibration has been elusive in the heavier nuclei. It is seen as a single state in ^{48}Ca, (Steffen, et al.,

1980), and as a broader bump in ^{90}Zr(p,p') (Anantaraman, et al., 1981). However, the total amount of strength found is small compared to the shell model expectations. The excitation energy of the state is not much different from the Gamow-Teller state, but the widths found are much smaller. One reason for this is that the residual nuclei are quite different in the two cases. In one case it is an even-even nucleus with a low level density, to be contrasted with the high level density odd-odd nucleus in the other case.

IV. THEORETICAL CONSIDERATIONS

A. The calculation of widths

A simple theory for the width of excitation can be based on powers of the Hamiltonian. Given an operator $\mathcal{O}$, the first two Hamiltonian moments are defined

$$\bar{E} = \frac{\langle \mathcal{O} H \mathcal{O} \rangle}{\langle \mathcal{O} \mathcal{O} \rangle} \tag{14}$$

$$\sigma^2 = \frac{\langle \mathcal{O} (H-\bar{E})^2 \mathcal{O} \rangle}{\langle \mathcal{O} \mathcal{O} \rangle} \ . \tag{15}$$

The variance σ^2 provides a measure of the width of the strength function for the operator $\mathcal{O}$. The technique of moment expansion has been applied to shell model studies in other contexts, and is described by (French, et al., 1978). On the question of damping of single-particle motion, the variance σ^2 was first estimated by Lane, Thomas and Wigner, (1955). They considered a nucleon in an infinite Fermi sea, interacting with the other particles by a Yukawa force of realistic strength and range. A very large value was found for the variance,

$$\sigma \sim 22.5 \text{ MeV} \tag{16}$$

As we saw in previous sections, empirical widths are much smaller. Indeed, if the σ of eq. (15) is interpreted as a width there would be little trace of shell structure in the strength functions. The resolution of this contradiction is seen upon recalling that the empirical widths are the widths of the observed peaks at the half maximum points. Any small contributions to the strength function

at high energy are irrelevant to the width. Unfortunately, the variance is very sensitive to the distant wings of the strength distribution. Thus σ is not useful in large Hamiltonian spaces.

We really want to calculate the spreading of the strength to nearby states, which of course may be done by diagonalizing the Hamiltonian. Providing the only off-diagonal parts of the Hamiltonian are the matrix elements between the simple excitation and the background states, the exact strength function can be calculated algebraically, as outlined in Appendix A. One can further obtain simple analytic formulas for the strength distribution by averaging the strength over some interval. In the simplest approximation, one assumes constant Hamiltonian matrix elements and equally spaced background states. The averaging then gives the familiar Breit-Wigner distribution

$$S(E) = \frac{S_0}{2\pi} \frac{\Gamma^{\downarrow}}{(E-E_0)^2 + (\Gamma^{\downarrow}/2)^2} \tag{17}$$

Here S_0 is the integrated strength, and the width $\Gamma^{\downarrow}$ is given by Fermi's Golden Rule,

$$\Gamma^{\downarrow} = 2\pi V^2 \frac{dn_f}{dE} \tag{18}$$

In eq. (18), V is the interaction between the simple state and a background state, and dn_f/dE is the density of background states.

It can be shown that

$$A(t) = \int \frac{S(E)}{E_0} e^{-iEt} \, dE = e^{-\frac{1}{2}\Gamma^{\downarrow} t} e^{-iE_0 t} \tag{19}$$

is the time-dependent amplitude of the excitation. The corresponding probability then displays an exponential decay in time at

a rate $\Gamma^{\downarrow}$,

$$|A(t)|^2 \equiv P(t) = e^{-\Gamma^{\downarrow} t} \tag{20}$$

Exponential decay, being time-irreversible, may seem to be in contradiction to the underlying physics based on a time-reversible Hamiltonian. The resolution of the paradox is that we have computed an average quantity, and the averaging (coarse-graining in statistical mechanics) destroys the reversibility of the equations.

The generalization of the Breit-Wigner distribution to non-uniform conditions, given in Appendix A, is just what would be expected intuitively. In eq. (17), $\Gamma^{\downarrow}$ becomes an energy-dependent width $\Gamma(E)$. It is evaluated by an equation similar to eq. (18) with state-dependent matrix elements and averaged level densities replacing the constants. There is also an energy shift in the $(E - E_0)$ term in eq. (17). We will not discuss this shift, except to mention that it is implicitly contained in calculations based on diagonalizing the Hamiltonian, and that it can have a significant influence on the location of the peak of the strength function Traditionally, experimentalists fit their distributions to Gaussian functions,[†] although there is no theoretical justification for such

[†] The variance of the Gaussian σ^2, which is often quoted, is related to the width (full width at half maximum) by

$$\Gamma^{\downarrow}_{FWHM} = \sqrt{8 \ln 2}\ \sigma = 2.35\sigma .$$

For a Breit-Wigner distribution σ is of course infinite, because in deriving the distribution one has assumed an infinite number of states coupling to the initial one with a fixed strength.

a form. The suppression of the strength function wings in a Gaussian fit means that there will be a tendency to underestimate the total strength associated with the peak. It is important to use the best possible functional forms, when attempting to extract a total strength of a peak that is partly obscured by a poorly-understood background.

We saw in Sec. III the Lorentzian distribution, eq. (13), applied to the strength function. The Lorentzian function is asymmetric about the peak, with the low-energy wing suppressed, and this behavior is often found in empirical strength distributions. The asymmetric energy dependence of the Lorentzian has two sources. First, a classical oscillator damped by a linear frictional force has a dipole strength function of the form eq. (17) with $\Gamma^{\downarrow}$ proportional to E at low energies. As we will see later, the width in many-body theory is strongly energy dependent. There is, however, no real justification for assuming a linear energy dependence for $\Gamma(E)$, although it does give a fit to more microscopic calculations over a limited energy regime. Second, the photon coupling to a state of given dipole matrix element has a strength proportional to the photon energy. This source of energy dependence in the Lorentzian is peculiar to radiative damping, and should not be present in other kinds of damping. Like the Breit-Wigner distribution, the Lorentzian has an infinite σ.

B. The nuclear response in RPA

The mean-field theory of nuclear motion, RPA, has been remarkably successful for describing vibrational properties (cf. e.g. Bertsch and Tsai, 1975; Broglia, et al., 1971; Ring and Speth, 1974; Liu and Brown, 1976; Blaizot and Gogny, 1977). We wish to

summarize the results of RPA here for two reasons. First, vibrational motion can be damped already in the mean field theory, and we need to see how important this actually is for the vibrations under consideration. Second, the coupling of nucleons to the internal degrees of freedom of the nucleus, a central problem of damping theory, is closely related to the coupling of external fields to the nucleus, which the RPA treats.

Early RPA calculations were based on quite schematic interactions and small configuration spaces for the particle-hole wavefunctions. Consequently the models did not have great predictive power, although qualitative features of the strength functions were readily reproduced. The recent progress is due to two improvements in the model. First, the use of large configuration spaces makes it possible to calculate absolute transition strengths, if the interaction is known or is adjusted to fit vibrational frequencies (Broglia, et al., 1971, Ring and Speth, 1974). The energy-weighted sum rules are only satisfied in large-space calculations. The second advance in RPA is the use of self-consistent interactions derived from Hartree-Fock models. The requirement that the Hartree-Fock theory reproduces ground-state properties strongly constrains the interaction and the derived theoretical response. In the self-consistent theory, the energy-weighted sum rules are automatically satisfied. This is a constraint on the strength function mainly at high energies. The predicted low-frequency collective states generally also show agreement with experiment. Thus the theory provides a useful description of the entire response function.

The importance of the interaction to the response may be

seen qualitatively from the static polarizability. This is defined as

$$\Pi(0) = 2\sum_i \frac{\langle 0|Q|i\rangle^2}{E_i} \qquad (21)$$

where Q is the external field. The first estimate of this would be from the independent particle model, in which the states i would be particle-hole states, with excitation energy given by the Hartree-Fock single-particle energies. A classic argument by Mottelson (1960) shows that the isoscalar quadrupole polarizability is enhanced by a factor of two over the independent particle value, if self-consistency is imposed on the interaction. The difference in strength functions for RPA and the independent particle model may be seen in Figs. 16 and 17. The low-frequency strength is minute in the independent-particle model, but the interaction induces a strong vibration at low frequency. In the case of the octupole response, the strength below 5 MeV excitation is increased by a factor of 10 by the interaction. It is clear that the damping of low-energy excitations will be very much influenced by the low collective vibrations.

Because of the basic characteristics of the nuclear interaction, short-range and attractive, only the isoscalar density response is enhanced at low energies by the interaction. In all other channels, the interaction is repulsive and the response is suppressed at low energies. We illustrate this with the isovector dipole response calculated in ^{208}Pb, Fig. 18. This calculation treats the particle continuum exactly, so the widths of the

individual peaks are theoretical escape widths, $\Gamma^{\uparrow}$. We see that the widths of the individual peaks are small, in agreement with the experimental finding that escape widths are unimportant in heavy nuclei. We also see that the dipole strength is spread over many particle-hole components. The spreading within the space of particle-hole configurations is known as Landau damping in infinite media. However, this damping behaves quite differently in finite systems than in infinite systems. Infinite systems exhibit Landau damping mainly for channels with an attractive interaction, but the nucleus has no spreading to nearby particle-hole states for the giant vibrations in the attractive isoscalar channel (see Fig. 16). Conversely, the isovector channel would have an undamped mode in the infinite system, while the nuclear isovector dipole is predicted to spread as in Fig. 18. However, there are probably defects in the isovector interaction in the calculation of Fig. 18. The experimental strength is concentrated at a somewhat higher energy, and probably is not Landau-damped.

So far we have said little about the details of the RPA theory. The RPA response can be calculated treating the full complexity of the nucleon-nucleon interaction, but the results just confirm the validity of more simplified treatments. The structure of the collective states turns out to be very simple, as far as the coupling to external fields is concerned. To an excellent approximation, the transition density for isoscalar collective states of angular momentum $L \neq 0$ is given by the macroscopic model,

$$\delta\rho(\vec{r}) \equiv \langle 0|\hat{\rho}|i\rangle \simeq \frac{\beta R}{\sqrt{2L+1}} \left.\frac{d\rho_0}{dr}\right|_r Y_{LM}(\hat{r}) \qquad (22)$$

where ρ_0 is the ground state density and βR characterizes the strength of the coupling. Notice that the vibration is peaked on the surface, because of the derivative in eq. (21). The coupling of the collective state to particles can be described with a transition potential,

$$\delta U(\vec{r}) \equiv \langle o|v(\vec{r}-\vec{r}')|i\rangle \qquad (23)$$

A simple treatment of this potential which has the necessary self-consistency assumes that the transition potential is related to the static potential U_0 in the same way as the transition density is related to the static density,

$$\delta U(\vec{r}) \simeq \frac{\beta R}{\sqrt{2L+1}} \left.\frac{dU_0}{dr}\right|_r Y_{LM}(\hat{r}) \qquad (24)$$

Of course this is an approximation, derivable only from zero-range interactions. A finite range would preserve the same radial dependence, but would give an additional L-dependence to the transition potential, cutting it off for high L.

In Brueckner theory, the extracted Hartree-Fock field is non-local, i.e. strongly momentum-dependent. In principle, this momentum dependence will have an effect on the transition potential, eq. (23), but this should not play much role for low-energy vibrations. When the momentum dependence is omitted from the transition potential in the RPA calculations, the field must be renormalized by about 20% to achieve self-consistency. It is a remarkable feature of the collective vibrations, that their properties are

rather independent of the details of the interaction used in the RPA theory (cf. Bertsch and Tsai, 1975). The simple form for the collective state coupling, eqs. (22) and (23), was anticipated in the early work of Bohr (1952), who assumed that the transition fields would take this form, and normalized the deformation parameter βR to the known experimental data.

V. THEORY OF SINGLE-PARTICLE DAMPING

In many-body theory, it is conventional to formulate the damping problem in terms of the self-energy of an excitation. We first define the Green's function for an excitation. This may be expressed

$$G(E) = \frac{1}{E-e_{HF}-\Sigma(E)+i\varepsilon} \tag{25}$$

where e_{HF} is the energy of the particle in the Hartree-Fock Hamiltonian, and Σ is the self-energy, to be calculated by a perturbation expansion. The damping width of the state is given by

$$\Gamma^{\downarrow} = 2 \text{ Im } \Sigma, \tag{26}$$

where Σ is evaluated at a complex energy $= E + i\Delta$, and Δ is a suitable averaging interval. In an optical model description of a particle state, Im Σ is equal to the expectation of the imaginary optical potential,

$$\text{Im } \Sigma = \langle W \rangle \tag{27}$$

giving a simple formula to relate the optical model absorption to the damping width,

$$\Gamma^{\downarrow} = 2\langle W \rangle \tag{28}$$

Eq. (26) may be evaluated in lowest order perturbation theory as

$$\Gamma^{\downarrow} = 2 \text{ V Im } \frac{1}{H-E+i\Delta} \text{ V} \tag{29a}$$

$$\approx 2 \sum_{\alpha} |\langle a|V|\alpha\rangle|^2 \frac{\Delta}{(E_{\alpha}-E)^2+\Delta^2} \tag{29b}$$

$$\approx 2\pi \overline{|\langle a|V|\alpha\rangle|^2} \frac{dn_f}{dE} \tag{29c}$$

The last step follows if the interval Δ is large compared to the spacing of levels α. Thus we recover exactly the simple-minded Golden Rule expression, eq. (18). In perturbation theory, a specific form is assumed for the background states α, namely these are the 2 particle-1 hole states which interact with the single-particle excitation.

One elementary point that may cause confusion is the relation between the imaginary optical potential and the mean free path λ (Negele and Yazaki, 1981; Fantoni, et al., 1981). From eq. (29) we see that the imaginary optical potential is directly related to the width or its reciprocal, the mean life of the state,

$$\frac{1}{\tau} = \Gamma^{\downarrow} = 2\langle W \rangle \tag{30}$$

The mean free path can be defined as the decay length for a wave function that is stationary in time. Representing the wave function as $\exp(ik_R r - k_I r)$, the mean free path is

$$\lambda = \frac{1}{2k_I} \tag{31}$$

We find k_I by demanding that the expectation of the Hamiltonian have a vanishing imaginary part. With the kinetic part of the Hamiltonian given by $k^2/2\tilde{m}$, where $\tilde{m}$ is the effective mass associated with the nonlocality of the Hartree-Fock potential, we find

$$\frac{k_R k_I}{\tilde{m}} = W \tag{32}$$

Thus the relation between mean free path and decay time is

$$\frac{\lambda}{\tau} = \frac{k_R}{\tilde{m}} \tag{33}$$

This is nothing more than the group velocity of the particle, as we expect from classical arguments. The appearance of the effective mass in eq. (33) means that one has to be careful about relating damping data based on energy widths to data based on spatial attentuation, since the relation involves an assumption about the effective mass.

A. Infinite nuclear matter

Equation (29) is easily evaluated for particles near the Fermi surface in an infinite Fermi gas. The density of 2 particle-1 hole states having a given total momentum k near k_f may be expressed (Jeukenne, et al., 1976)

$$\frac{dn}{dE} = \int dp dp' dh \, \frac{n_h}{(2\pi)^9} (1-n_p)(1-n_{p'})(2\pi)^3 \delta^3(k_p + k_{p'} - k_h - k) \delta(E + \varepsilon_h - \varepsilon_{p'} - \varepsilon_p)$$

$$\cong \frac{1}{(2\pi)^4} (\tilde{m}^3)(E-\varepsilon_F)^2 \tag{34}$$

In the first equation, the n's are the occupation numbers of the single-particle states, and the wave function normalization is one particle per unit volume. In the second line, $\tilde{m}$ is the effective mass of the particles in the Hartree-Fock Hamiltonian, and ε_F is the Fermi energy. Then the width of a single-particle states is given by

$$\Gamma^{\downarrow} = \frac{1}{(2\pi)^3} (\tilde{m})^3 (E-\varepsilon_F)^2 \bar{V}^2 \tag{35}$$

Here V is an average matrix element of the interaction between plane-wave states, having dimensions of a volume integral. An important feature of eq. (35), arising from the density of states, is the quadratic dependence on excitation energy (Brueckner, et al., 1955).

For the approximation in eq. (34) to be valid, the excitation energy should be much smaller than the Fermi energy (37 MeV). The quadratic dependence at low energies was used in the phenomenological parameterizations of the single particle width in eq. (7). Orland and Schaeffer (1978) have also suggested a parameterization to extend beyond the region of quadratic energy dependence.

Second-order perturbation theory is not an adequate approximation for nuclear systems. The interaction is quite strong, and the induced correlations must be explicitly included in the calculation of matrix elements. A simple soluble example is given by the Fermi gas with hard-core repulsive interactions. The particle-self energy is infinite in second-order perturbation theory. With correlations included, the damping of a particle near the Fermi surface is finite and in the dilute limit is (Galitskii, 1958)

$$\Gamma^{\downarrow} = \frac{\hbar^2 k_F^2}{2m} \frac{2}{\pi} (k_F a) \left(\frac{k_F - k}{k_F}\right)^2 . \qquad (36)$$

Here a is the hard core radius. The correlation effects with realistic interactions may be treated by a number of techniques. The Brueckner theory has been used in several studies of the single-particle damping (Jeukenne, et al., 1976; Brieva and Rook, 1977). Jeukenne and collaborators calculated the nucleon self-energy of Brueckner theory using the Reid hard core potential. The imaginary part of their self-energy is shown in Fig. 19, as a function of excitation energy. The calculation was done for two values of the Fermi momentum, corresponding to nuclear matter density and roughly half nuclear matter density. From their numerical results the following conclusions may be drawn.

(1) The quadratic formula, eq. (32), is valid only for quite small excitation energies. In the low density calculation, the imaginary self-energy is almost constant above 20 MeV of excitation.

(2) Below 60 MeV of excitation, the imaginary self-energy is larger in low density nuclear matter than at saturation density. This suggests that the absorption is enhanced on the surface. As we saw above, this is just how the empirical optical potential behaves.

(3) The main contribution to the imaginary self-energy for the low density case is from nucleon-nucleon scattering in the $^3S_1 - ^3D_1$ partial waves. The $^1S_0$ has only about one-third the contribution, and other partial waves are negligible. In fact it is the large $^3S_1$ phase shift and not the mixing between $^3S_1$ and $^3D_1$ that is responsible for the $^1S_1 - ^3D_1$ contribution. Thus to a good approximation, only the central interaction is responsible for the damping. At saturation density, the P waves become significant, and the spin couplings are important.

Figure 19 shows a direct comparison of the theoretical absorptive potential of Jeukenne, et al., and the empirical potential of Rapaport, et al., (1979). Between threshold and 15 MeV neutron energy, the empirical potential is surface peaked, and its maximum depth agrees closely with the Jeukenne et al. (1976) potential at half density. Above 15 MeV neutron energy, the empirical potential has an increasing volume contribution, in agreement with the theory.

B. Finite nuclei

The agreement between the empirical optical potential and the theory based on infinite nuclear matter should not be taken too seriously, because there is no justification for treating the

surface as low density nuclear matter. Especially for low excitation energies, one needs a better description of the doorway states than the infinite nuclear matter theory provides. The simplest hypothesis is that the doorway states for single-particle excitations are the 2 particle-1 hole shell model states of a single-particle Hamiltonian. An early study along these lines was a calculation of the neutron strength function in Sn and Pb isotopes by Shakin (1963). He determined the single-particle levels from a phenomenological Hamiltonian, and found the 2p-1h states that should be near the neutron threshold. The mixing of these states with the continuum s-wave neutron was then calculated with a simplified interaction. The predicted strength function does not agree in detail with the empirical, but the order of magnitude is correct. The limited agreement is perhaps surprising; as was pointed out by G.E. Brown and others, the correlations and energy shifts associated with the particle-hole interaction should modify the damping substantially. Subsequent calculations in finite nuclei include these correlation effects, treating the low-lying vibrations explicitly.

The damping by vibrational excitation may be calculated from eq. (29), using eq. (24) for the coupling between the particle and the vibration (cf Fig. 20). The basic matrix element is

$$\langle\gamma|V|LM,\alpha\rangle \cong \frac{\beta}{\sqrt{2L+1}} \int d^3r\ \psi_\gamma(\vec{r})\ \frac{RdU_0(r)}{dr}\ Y_{LM}(\hat{r})\psi_\alpha(\vec{r}). \qquad (37)$$

In this equation, ψ are the single-particle wave functions. The coupling strength β is to be determined either from a microscopic RPA calculation, or by the empirical data. The matrix elements

exciting the different M states of the vibration can be combined into a single matrix element to the state with angular momenta j_α and L coupled to total j_γ. The j-coupled matrix element is given by

$$\langle\gamma|V|(L\alpha)j_\gamma\rangle = \frac{\beta_L}{\sqrt{(2L+1)(2j_\gamma+1)}}\ \langle j_\gamma|R\frac{dU_0}{dr}|j_\alpha\rangle\langle j_\gamma\|Y_L\|j_\alpha\rangle \qquad (38)$$

We have separated out the radial integral of the transition potential

$$\langle j_\gamma|R\frac{dU_0}{dr}|j_\alpha\rangle = \int r^2dr\phi_\gamma(r)\ R\frac{dU_0}{dr}\phi_\alpha(r) \qquad (39)$$

and the reduced matrix element of a spherical harmonic, defined in eq. (B3). Given the vibrational properties of the nucleus and the single-particle Hamiltonian, it is now straightforward to calculate the damping. Before we discuss the results of the calculations, one difficulty of principle should be mentioned. The exchanged interaction is implicit in the potential field and thus in the vibrational coupling potential. As is well known in many-body theory, this leads to an overcounting of the perturbation graphs in second order. The remedy is to subtract the perturbation graph of Fig. 20B from the self-energy associated with the particle-vibration coupling, Fig. 20a. The contribution of Fig. 20b can be

easily estimated by replacing the RPA response in Fig. 20a by the noninteracting particle response. It is found that for the damping of low energy excitations, the graphs 20b are negligible compared to 20a (Bertsch, et al., 1979), as is expected from the discussion of Sec. IVB.

1. The optical potential

There have been a number of calculations of the optical potential in finite nuclei based on the particle-vibration doorway hypothesis. Since the transition densities of the collective states peak on the surface, the derived imaginary optical potential will also have this property. We saw from the empirical potentials and the Brueckner calculations that above about 20 MeV excitation the volume absorption becomes dominant. Thus we expect the vibrational treatment to become inadequate for higher energies. This is indeed found to be the case in the reported calculations. For example: Rao, Reeves and Satchler (1973) calculated the optical potential for 30 MeV proton scattering from ^{40}Ca and ^{209}Pb in the particle-vibration doorway model and found that only 3/4 of the absorptive cross section could be accounted for. The inadequacy of the particle-vibration doorways at these energies has been confirmed by Bernard and Van Giai (1979), by Osterfeld, et al., (1981), and by Bouyssy, et al., (1981), who describe the vibrations microscopically and treat the coupling with the Skyrme Hamiltonian. Bernard and Van Giai obtained a theoretical volume integral of the absorption in ^{209}Pb which was only 1/4 of the empirical; Bouyssy, et al., obtained half the empirical volume integral in ^{40}Ca. Coulter and Satchler (1977) included additional doorways in the absorption with the (p,d) pickup reaction channels. However, this did not remedy the situation; the

calculated surface absorption was still only half the empirical.

Several calculations have been reported for the optical potential at low excitation energies (O'Dwyer, et al., 1972), (Lev, et al., 1973). A serious problem that arises in any theory here is that the density of doorway states is very low. Consequently, a large averaging interval must be used in eq. (20b) to produce a smooth potential. In such situations, it is better to compare with the actual strength functions than to smooth out structure which is predicted to survive. Indeed, the empirical neutron strength function shows large fluctuations from nucleus to nucleus (Fig. 4).

2. Neutron strength function

The neutron strength function has been studied in the particle-vibration doorway model by a number of authors. As mentioned above, in many cases the density of doorway states is too low to make a definitive comparison with experiment. With a low density of states, the results are sensitive to the averaging interval in the calculated damping. Thus the problem of understanding the damping is shifted to the spreading of the doorway states themselves. Nevertheless, qualitative conclusions may be drawn from existing calculations. One recent calculation which compared theory and experiment was that of Dambasuren, et al. (1976). These authors calculated the s- and p-wave strength function in the mass region $A \sim 120$. The single particle Hamiltonian was based on an empirical Woods-Saxon potential. The vibrations included are mainly the 2^+ and 3^- collective states, with the interaction strength chosen to reproduce the excitation energy of the states in RPA. The authors

find very little spreading of the strength away from the single-particle energy. In the case of the s-wave, the single-particle energy is bound by about 4 MeV, and the strength predicted in the neutron resonance region is underpredicted. This is despite the fact that the empirical strength function already has a deep minimum in this mass region (see Fig. 4). Conversely, the p-wave orbit is near zero binding, and its strength is overpredicted in the calculation. It might be thought that the lack of agreement could be attributed to the restriction of the doorway vibrations to low multipolarities. However, more extensive calculations discussed below give similar results.

3. Deeply-bound hole states

Following the measurements of the $g_{9/2}$ hole strength in the Sn isotopes, Koehling and Iachello (1978) applied the particle-vibration doorway model to this data. They used single-particle energies from a Woods-Saxon potential, and vibrational couplings fixed by the energies of the low collective states. Only L = 2 and L = 3 multipoles were considered for the vibrational states. The calculation predicted far too little damping, with the $g_{9/2}$ strength split into only two large components. Both components were predicted to be in a region of the spectrum where only one quarter of the possible strength was found.

A later calculation by Soloviev, et al., (1980) included the full spectrum of vibrations, finding that the widths were significantly increased. These authors reported their theoretical spreading widths in a way that was directly comparable to experiment. They

computed the dispersion in the strength contained within some fixed energy interval, and reported the amount of strength in the interval as well as the dispersion. In many cases they find agreement with experiment. However, problems still remain with the strength in the heavier Sn isotopes, with more concentration of strength predicted at low excitation than is observed.

This difficulty was partly overcome in a recent calculation by Bortignon and Broglia (1981b) who use a Hartree-Fock single-particle Hamiltonian rather than the Woods-Saxon. The result is a higher center of gravity for the $g_{9/2}$ strength. The vibrational coupling is self-consistent, and so should be equivalent to previous treatments. The amount of $g_{9/2}$ strength at low energy then comes out to 25%, in agreement with experiment (Gerlic, et al., 1980; Siemssen, et al., 1981). The calculation predicts also a relatively narrow high energy component, which does not seem to be consistent with the experimental findings (Siemssen, et al., 1981).

A similar situation is found for the spreading of the $h_{11/2}$ hole in ^{207}Pb. Experimentally, the energy region between 7 and 10 MeV contains 40-70% of the total $h_{11/2}$ strength. Bortignon and Broglia agree with the dispersion of the strength in this region, but predict that it contains only 25% of the total. A large portion of the strength is predicted in a peak about 10 MeV. If the predicted strength distribution is correct, it is difficult to see why the upper peak was not observed. The presence of the high energy components is connected with the small effective mass ($\tilde{m}/m = 0.76$) in the Hartree-Fock Hamiltonian and provides an important test of the Hamiltonian.

4. An adiabatic model

Before concluding the discussion of single-particle damping, we wish to point out a limit in which the damping can be easily estimated. One makes the adiabatic assumption that the vibrational energy is small compared to other energies. Then the single-particle strength is strongly mixed with the vibrations, and the variance becomes a useful measure. The variance is evaluated from the summed squares of the interaction matrix elements, eq. (38),

$$\sigma^2 = \sum_{\gamma,i,L} \beta_L^2(i) \langle j_\gamma | R \frac{\partial U}{\partial R} | j_\alpha \rangle^2 \frac{\langle j_\alpha \frac{1}{2} L0 | j_\gamma \frac{1}{2} \rangle^2}{4\pi} \qquad (40)$$

The average value of the radial matrix element is of the order of 50 MeV. The Clebsch-Gordan coefficient asymptotically has the value $P_L(j/2) \approx -\frac{1}{2}$ for $L = 2$. Estimating the average number of states γ in the major shell that can couple to the initial state α to be 3, we find for the low energy quadrupole vibrations a dispersion

$$\sigma^2 \approx \beta^2 (12 \text{ MeV})^2 \qquad (41)$$

Typical values of β are 0.1, leading to a damping width

$$\Gamma^\downarrow \approx 2.4\sigma \approx 3 \text{ MeV} \qquad (42)$$

This is certainly the right order of magnitude to explain the damping of the low-energy particle excitations, and the fluctuations from nucleus to nucleus associated with the low-lying vibrations.

As a general conclusion we see that the particle-vibration coupling gives the right order of magnitude for the damping width of excitations near the Fermi surface. However, there is an overall tendency for the theoretical calculations to underpredict the empirical spreading. A full understanding must await better experiments that can locate the missing strength of the more highly excited single-particle states (cf. e.g. Siemssen, et al., 1981).

5. Energy dependence of damping

It is instructive to examine the energy dependence of the damping width in the particle + vibration model, eq. (A10), for several reasons. We would like to know the accuracy of the infinite Fermi gas result, eq. (35), that $\Gamma(E) \propto E^2$. Also the energy dependence of the real part of the self-energy, interesting in its own right, is intimately connected to $\Gamma(E)$ via a dispersion relation. An example of $\Gamma(E)$ is shown in Fig. 21, for the $s_{1/2}$ orbit in ^{208}Pb (Bertsch, et al., 1979). We see that there is a rather sudden onset of damping at $E \approx 5$ MeV. This is due to the opening of the doorways involving low-lying vibrations. There is a plateau up to about 10 MeV, where another set of doorways associated with giant vibrations begins to open up. Similar results are found for other orbitals, and in other calculations based on the particle + vibration model (Wambach, et al., 1981). It is apparent that the shell structure and the collective behavior of vibrations completely destroy the simple functional form of the energy dependence from eq. (35). The predicted energy dependence looks more like a series of steps, and this accords much better with the empirical widths of Table I.

The fact that the width is small for low energies means that the doorway treatment will fail for calculating widths of the more complicated configurations, since these do not have much energy available to create additional vibrations. Thus the problem of understanding the widths of the doorways themselves is completely unresolved at this time.

VI. THEORY OF VIBRATIONAL DAMPING

The starting point for the calculation of vibrational damping is to expand the vibrational wave function in particle-hole components. It is then natural to treat the damping via doorway states of 2-particle 2-hole structure (Danos and Greiner, 1965). This approach has two drawbacks. First, one needs a priori knowledge of the interaction to extract a meaningful width. Second, the collectivity of the vibrational doorways should not be neglected, as was seen in the single-particle damping. These problems are sidestepped if one takes a less ambitious approach. Rather than calculate the damping of the vibrations explicitly, one can simply use theory to relate it to the damping of the particle and hole of which it is composed.

A. Independent particle-hole model

A naive model of the damping is based on the assumption that the particle and hole decay independently. For a single component wave function, the damping would be

$$\Gamma^{\downarrow}_{ph} = \Gamma^{\downarrow}_{p} + \Gamma^{\downarrow}_{h} \tag{43}$$

This formula needs some further definition because of the energy dependence of the damping, and because the vibrational states are made up of many particle-hole configurations. The damping is roughly independent of configuration, but can depend strongly on the energy available to the particle or hole orbital. The energy available is the total vibrational energy, less the excitation energy of the spectator orbital with respect to the Fermi surface.

For the important configurations of the giant dipole, this energy is typically more than half of the dipole vibrational energy, ranging from ∿12 MeV in medium nuclei to ∿8 MeV in ^{208}Pb. Taking the single particle width from eq. (4), the predicted dipole width then varies from ∿10 MeV in medium nuclei to ∿5 MeV in ^{208}Pb. The independent decay model was applied in a detailed calculation by Dover, et al., (1972), on the damping of the ^{208}Pb dipole state. The single-particle damping was deduced from various optical potentials of n + ^{208}Pb. The single particle widths were found to be in the range 1-3 MeV, giving a dipole damping of 2-6 MeV, which brackets the empirical value of 4 MeV. However, the transfer reaction data in Table I suggests that the single particle widths should be larger, in which case the dipole spreading would be predicted to be too large.

B. Coherence of particle-hole excitations

The coherence between particle and hole in a collective state can drastically modify and reduce the damping as calculated in eq. (43). An example from another field of physics is the plasmon excitation of a metal. This collective electron particle-hole state can have a width of 0.2 eV at an excitation energy of 10 eV. Single-particle excitations at the same excitation energy would have widths of several eV. The reduction of the damping arises very naturally in a theory which includes all the second-order damping processes coherently (Dubois, 1959).

It can be shown on quite general grounds that there is a strong suppression of the coupling to two-particle two-hole states in infinite Fermi systems, when the momentum of the collective state goes to zero (Pines and Nozieres, 1966). The same reduction

is built into the quantum collision integral in the Landau theory of collective vibrations. This is shown in Appendix C.

A theory of the damping that respects the coherence of particle and hole is indicated with the perturbation graphs of Fig. 22. The first two graphs on the right-hand side represent the contribution to $\Gamma^{\downarrow}_{coll}$ arising from the separate widths of the particle and hole, evaluated at the collective state energy, as in eq. (43). The other two graphs may be viewed as vertex corrections to the self-energy of the collective state. They typically interfere destructively and reduce the total width. The physical origin of the cancellation is clear from the amplitude sum on the left-hand side of Fig. 22. The particle and hole usually couple to other degrees of freedom with opposite signs, so the total coupling is reduced. For example, the quadrupole moment of a collective state is small, and so the coupling to quadrupole vibrations would be weak. However, for coupling to degrees of freedom involving spin and isospin, the interference can have a positive sign. For example, a spin-flip collective state would have the spin of the particle added to that of the hole, and so it would couple more strongly to the other spin degrees of freedom in the nucleons. The general formula relating the vertex correction diagrams to the single-particle self-energy diagrams is given in Appendix B. The dependence of the interference on the spin and isospin quantum numbers is given by the factor

$$C(S',T')(-1)^{S+T}\begin{Bmatrix} \frac{1}{2} & \frac{1}{2} & S \\ \frac{1}{2} & \frac{1}{2} & S' \end{Bmatrix}\begin{Bmatrix} \frac{1}{2} & \frac{1}{2} & T \\ \frac{1}{2} & \frac{1}{2} & T' \end{Bmatrix} \tag{44}$$

where we have designated the vibrational quantum numbers by S,T, and the quantum numbers of the excitation in the doorway by S', T'. The factor C relates the particle-particle to the hole-hole matrix elements. The sign of this expression is given in Table III for the various possible spin-isospin combinations. We see, in agreement with the qualitative arguments above, that the sign is always negative if the intermediate vibration has S' = T' = 0. Also, if the collective state is scalar in spin and isospin, the cancellation is maintained for any kind of doorway vibration.

The complete formula for the vertex correction, eq. (B9),(B16), also requires a recoupling of the orbital angular momentum with the factor

$$(-1)^{\ell_k+\ell_i+\lambda}\begin{Bmatrix} \ell_k & \ell_i & \lambda \\ \ell_i, & \ell_k, & \lambda' \end{Bmatrix} \tag{45}$$

In the classical limits, this 6-j symbol is given by (Edmonds, 1960)

$$(-1)^{\ell_k+\ell_i+\lambda}\begin{Bmatrix} \ell_k & \ell_i & \lambda \\ \ell_i, & \ell_k, & \lambda' \end{Bmatrix} \cong \sqrt{2\ell_i+1)\,(2\ell_k+1)}\;\frac{1}{\lambda}\left(1+\mathcal{O}\left(\frac{1}{\lambda}\right)\right) \tag{46}$$

providing $\ell_i, - \ell_i, = \ell_k - \ell_k$

Thus the sign of the interference depends entirely on the spin-isospin structure of the graph. The collectivity of the giant modes insures that the different particle-hole amplitudes in eqs. (B8,9) are of the same order of magnitude.

The first model calculation incorporating the coherence were quite schematic. Bertsch (1971) assumed doorways of 2p-2h structure with S' = T' = 0 for the excited p-h pair, and found that the width of the giant dipole would be reduced below the single-particle width. A model of the isoscalar quadrupole vibration

based on a schematic interaction was studied by Ui (1975). He found a complete destructive interference with his interaction, indicating the need for a more detailed theory. Before describing the more detailed calculations, we discuss how the adiabatic model fits into this framework.

C. The adiabatic model

An alternative description of the damping treats the vibrational coupling in the adiabatic approximation. We saw before how the single particle motion is damped by the quadrupole vibrations in this approximation, eqs. (40-42). The same model can be applied to particle-hole excitations. One determines an effective coupling between the collective state and the vibrations by studying how the energy of the collective state depends on deformation. The following result is obtained for the giant dipole state (Bohr and Mottelson, 1975):

$$\sigma^2 = 0.2\ \beta^2 (\hbar\omega_D)^2 = \beta^2 \left(\frac{35\ \text{MeV}}{A^{1/3}}\right)^2 \qquad (47)$$

where ω_D is the dipole frequency and β is the quadrupole transition moment. This width is considerably smaller than the same model gives for the single-particle width. This can be understood in the particle-hole language as a cancellation effect between the particle and hole amplitudes. In the oscillator model, the ratio of the orbit coupling to the orbital energy is of the order of unity. The cancellation between particle and hole leads to a coupling of order $1/N$, N being the oscillator principal quantum number. The square of the matrix element for a collective state would thus behave asymptotically as $1/N^2 \sim A^{-2/3}$, in accordance with eq. (47).

D. Microscopic calculations

1. Light nuclei

In light nuclei, it is possible to calculate the damping of vibrations by explicitly constructing and diagonalizing the Hamiltonian matrix in the 1p-1h plus 2p-2h configuration space (Hoshino and Arima, 1976; Knüpfer, 1976; Adachi and Yoshida, 1978). Hoshino and Arima calculated the damping of the giant quadrupole vibration in ^{16}O and ^{40}Ca, and compared the exact Hamiltonian diagonalization with the perturbative approximations of Fig. 22. Their Hamiltonian was based on empirical single-particle energies, and a finite range residual interaction. In ^{16}O they found that the strength is distributed over 8 MeV. This is consistent with the experimental data, which shows a rather broad and flat strength distribution. Dehesa, et al. (1977) also calculated the quadrupole damping in ^{16}O, using RPA vibrations as doorways. They note that the 3^- vibration plays an important role in splitting the quadrupole strength. These authors only considered the coupling of the particle to the vibration, which in general is a dubious approximation. However, in analyzing the contributions to the spreading, Hoshino and Arima found almost no cancellation between particle and hole amplitudes. This happens because in the case of ^{16}O the coupling of the hole states is much more restricted by angular momentum than the coupling to the particle states.

In ^{40}Ca the hole orbits carry more angular momentum and Hoshino and Arima found a strong cancellation between particle and hole amplitudes. The net coupling strength to the 2p-2h doorways comes

out to a quarter of the strength from the self-energy graphs alone. The much narrower predicted strength distribution appears to agree well with experiment, which shows a width of 2.5 MeV for the quadrupole state. However, the agreement may be deceptive: more than 3/4 of the total strength is predicted to be in regions of the spectrum where only 45-60% is found experimentally. Hoshino and Arima note that their model predicts too little strength at very low excitation energy, where other degrees of freedom besides the 2p-2h doorways are important. Also, the shell space was probably inadequate to allow the full collectivity for the octupole doorway vibration.

2. Heavy nuclei

Microscopic calculations of heavier nuclei have been done by Dehesa, et al., (1977), by Soloviev, et al. (1977) and by Bortignon and Broglia (1981b). Soloviev, et al. use a formalism in which the particle-hole states are treated as boson excitations, i.e. phonons. The doorway states are the two-phonon excitations. The structure of the phonons is first computed in RPA. Then the coupling of a phonon to two phonons is evaluated by the perturbation expression corresponding to Fig. 23. It is found that the main contribution to the damping comes from doorways in which one of the phonons is a collective state and the other is noncollective. The noncollective states are essentially pure particle-hole configurations, so the model should be equivalent to other treatments that utilize particle-hole plus vibration for the doorways. The model was applied to the dipole and quadrupole strengths (Soloviev, et al., 1977), and to magnetic quadrupole strength

(Ponomarev, et al., 1979). The model Hamiltonian consists of a Woods-Saxon single-particle Hamiltonian, together with a separable residual interaction. The theoretical strength functions are displayed graphically, from which it is possible to extract a width. An example is the dipole state in ^{120}Sn, shown in Fig. 24. The theoretical strength function, averaged over an interval 1 MeV, has a FWHM of 2.5 MeV. The experimental width of the dipole state in ^{120}Sn is 4.9 MeV. Thus the theory gives the right order of magnitude, but tends to underpredict the value. This also happens for other nuclei with double closed shells. The calculation for the nonmagic nucleus ^{124}Te gave a much larger width, which is in better agreement with experiment.

Recently, Bortignon and Broglia (1981b) made a systematic study of the damping of the known giant vibrations for a range of closed shell nuclei, from ^{40}Ca to ^{208}Pb. They assume the doorways have the structure of particle-hole plus vibration, and use a single-particle Hamiltonian from the Skyrme III Hartree-Fock model, and a residual interaction of the self-consistent surface-coupling form, eqs. (37-39). The theoretical strength functions have a great deal of structure, making it difficult to extract a single width. The low-lying collective states dominate the damping, as was found in other calculations. Roughly 60% of the widths is due to these doorways. They find that the cancellation between particle

and hole amplitudes becomes more important in heavy nuclei. Fig. 25 shows an example of the distribution of coupling matrix elements for the giant quadrupole state in ^{208}Pb with and without the interference. We see roughly a factor of two cancellation, with a particularly large effect for the lower energy doorways. These components contain the collective 3^- vibration.

Bortignon and Broglia compare their strength functions with experiment by finding the variance of the strength within an energy interval. This procedure gives a width of 2.7 MeV, to be compared with the empirical 3 MeV width of the giant quadrupole in ^{208}Pb. Similar agreement is found for most of the other closed shell nuclei. However, the agreement may be illusory, if the electron scattering experiments turn out to be correct in the measurement of the total amount of strength in the peaks (Kühner, et al., 1981). According to theory, three-quarters of the total strength is in the giant vibration. This agrees with alpha particle scattering results, but as we noted earlier, the electron scattering indicates less than half of the strength is in the giant vibration region.

In the case of the monopole vibration, the theory definitely underpredicts the width. Bortignon and Broglia find that the monopole state is strongly collective in RPA calculations based on Hartree-Fock single-particle Hamiltonians. This strong collectivity, together with the fact that the $L = 0$ recoupling in eq. (15) produces an interference for all configurations, implies that the cancellation in Fig. 22 will be very strong. The theoretical width of the monopole comes out to be about 1 MeV, much

smaller than the empirical width of 3 MeV. The strong cancellation giving much too small a monopole width was also found in the recent calculation of Wambach, et al., (1982). These authors do not limit the doorway space to spin- and isospin scalar vibrations, but include a complete set of RPA modes. They find that less than 30% of the spreading arises from the additional doorways, giving confirmation to the surface-coupling model. They also found that the monopole state was predicted to be too narrow.

One possibility for explaining the large monopole width is that the escape widths might be much larger for a monopole vibration. The monopole transition density emphasizes the low-ℓ orbits, which have larger escape widths because of a reduced centrifugal barrier. A recent calculation by Van Giai and Sagawa (1981) predicts a 2 MeV escape width in ^{208}Pb. It would be interesting to measure the decay properties of the state, to confirm whether the width is in fact mostly escape.

The giant octupole mode is more strongly damped than the previous modes. It has a higher angular momentum, so the interference between particle and hole damping is reduced. It also lies at a higher energy, and so more doorways are available for decay. Bortignon and Broglia (1981a) calculate a width of about 8 MeV, which is consistent with the experimental analyses.

The recent elucidation of the Gmöw-Teller strength function permits the theory of the damping to be tested in the spin-isospin channel. Gaarde, et al., (1980) explicitly diagonalized a Hamiltonian matrix for 1p-1h and 2p-2h states in ^{48}Sc. Not only is the

overall width reproduced, but a correspondence can be seen between individual states of the theoretical calculation and concentrations of strength in the experimental distribution. The particle-hole plus vibration model gives good agreement with the 4 MeV experimental spreading found in heavier nuclei such as ^{90}Zr and ^{208}Pb (Bortignon, et al., 1982; Fiebig and Wambach, 1982). However, the observed peaks appear to contain only part of the total strength associated with the $\sigma\tau_-$ operator. In some experimental analyses, only one-third of the predicted strength is seen in the Gamow-Teller peak. Part of this missing strength has been ascribed to 2-particle nucleon-hole configurations, which mix with the ordinary particle-hole configurations to deplete the strength at low excitation energy. A significant amount of the missing strength may perhaps be found in the continuum background as discussed in recent calculations by Osterfeld (1982) and by Bertsch and Hamamoto (1982).

E. Macroscopic treatments of vibration damping

Attempts to systematize the trends in damping widths using classical notions of viscosity have been attempted by Auerbach and Yeverechyahu (1975) and by Nix and Sierk (1980). The classical viscous damping depends quadratically on the velocity field, which implies a quadratic dependence on the vibrational frequency. To derive the quantum behavior, one must study the collision integral in the Landau equation, as discussed in Appendix C. It is found that this integral depends quadratically on the energy available in the vibration, just as the single-particle damping

rate in infinite systems depends quadratically on the available energy. The experimental data show some tendency for a quadratic energy dependence, but the fluctuations from nucleus to nucleus are so strong that a macroscopic treatment must miss much of the physics. In our view, a model based on viscosity assumes that the damping is a bulk effect, arising in the nuclear interior, while the microscopic calculations show that the surface deformations play the dominant role in the damping.

VII. CONCLUSION

The general characteristics of particle damping are clear from the optical model descriptions of elastic scattering and the neutron strength function. There is a division between low energy excitations, say below 15 MeV, where the surface absorption dominates, and at energies above 25 MeV, where volume absorption starts to play an important role. Such behavior accords very well with theoretical expectations. The nuclear response at low excitation is dominated by surface degrees of freedom, and these couple strongly to the single-particle motion. In a pictorial language, one can say that the particles easily lose energy by bouncing inelastically from the nuclear surface. A consequence of this mechanism is the dramatic shell effects one sees in the systematics of the widths as a function of nuclear mass number. Closed shell nuclei are stiffer, i.e. have smaller transition strengths to low-lying collective states, and the damping is suppressed. The largest widths are found in the nuclei with strong collective states near the ground states.

For higher energy particle states, the theoretical studies confirm the importance of the volume absorption. The calculations based on the Brueckner theory give enough volume absorption, for particles up to 100 MeV in energy. However, there appear to be problems in describing the absorption in the surface region. Calculations of the surface absorption based on the RPA theory of the surface degrees of freedom give somewhat too small results. Perhaps the particle transfer degree of freedom, with the particle

forming a bound cluster with a nucleon from the target, will remove the discrepancy. This effect is implicit in the Brueckner calculation, which in principle treats the particle-particle correlations. This mechanism should be investigated also at low energy, where the surface degrees of freedom are often insufficient to explain the damping.

The surface coupling model often predicts much structure in the strength function. The most collective vibrations may split a substantial part of the strength away from the main peak. A study of the decay of the giant vibrations would be interesting to obtain more information concerning this point. The experimental strength function is typically quite smooth, and in order to reproduce this in the theory it is sometimes necessary to assume an unreasonably large damping of the doorway states themselves. There are other aspects of the data which suggest that the calculated damping may be too small. In exciting the giant vibrations and single particle states, one sees backgrounds that are not well understood. If the strength in the peak of the giant vibrations is less than 50% as suggested by some experiments, a much larger theoretical damping will be needed to reproduce the data.

The energy dependence of the damping has an analytic expression in the Fermi gas model with a quadratic energy dependence. However, because of the importance of the low-lying vibrations with energies of the order of 4 MeV, the actual damping sets in rather suddenly at these energies and does not increase much above 10 MeV. The volume part of the absorption seems to be quite constant

above a certain energy. In fact, all but the lowest energy damping can be characterized by an imaginary volume integral of about 100 MeV/nucleon.

We saw that there was a strong connection between single-particle damping and the damping of vibrational states, because the vibrations can be constructed from particle-hole configurations. With the main damping due to the surface deformations, the theory predicts a destructive interference between particle and hole contributions to the damping widths. A simplified model of the damping based on an adiabatic approximation also contains this effect. The interference between particles and holes helps explain why single particle states are seen as distinct peaks only up to about 8 MeV excitation, while collective vibrations are seen much higher. In the case of the monopole vibration, the cancellation appears to be much stronger than allowed by the experimental data. This question is not understood at present.

The surface coupling model has a number of successes, but is not quantitatively correct in several situations. Overall, the model describes the damping to better than a factor of two accuracy. If one would look for a systematic deviation of the model from the data, it is clear that the model does not give quite enough damping. Other degrees of freedom, not yet well understood, probably play a role in the damping.

ACKNOWLEDGEMENTS

We would like to acknowledge helpful discussions with A. Bohr, G. Crawley, C.H. Dasso, and B. Mottelson. We also thank the Institute for Theoretical Physics (Santa Barbara), the Niels Bohr Institute and Oak Ridge National Laboratory for support during part of this work. Financial support was received from the Danish Council of Research, the Fondazione della Riccia, the National Science Foundation under grants PHY-79-22054 and PHY77-27084, and the Department of Energy under contract W-7405-ENG-26 with the Union Carbide Corporation.

Table I. Single-Particle Widths

Orbital	Excitation Energy (MeV)	Width (MeV)	Source
$1h_{9/2}$ (π)	5.9	1.2	particle transfer (Gales, et al., 1982a)
$1g^{-1}_{9/2}$ (ν)	5.5	3.7	" " (Gales, et al., 1982b)
	6.6	3-4	" " (Siemssen, et al., 1981)
	7.5	4.9	" " (Gales, et al., 1982b)
$2f^{-1}_{7/2}$ (π)	6.8	3-4	" " (Stuirbrink, et al., 1980)
$1i_{13/2}$ (π)	7.6	4	" " (Gales, et al., 1982a)
$1h^{-1}_{11/2}$ (ν)	8.3	3.7	" " (Gales, et al., 1978)
$1f^{-1}_{5/2}$ (ν)	10.6	8	" " (Siemssen, et al., 1981)
$s_{1/2}$ (ν)	~8	4	neutron strength function (Mughabghab and Garber, 1973)
$4s_{1/2}$ (ν)	~15	3-4	neutron scattering (Rapaport, et al., 1979)
	>25	~15	nucleon scattering (see text, Eq. (12))
$1s^{-1}_{1/2}$ (π)	50	30	knockout reaction (Nakamura, et al., 1974)

Table II. Widths of Giant Vibrations

Vibration (λ^πL)	Width Heavy Nuclei	Width Light Nuclei	Source
Giant Dipole (011)	4	7	Berman and Fultz (1975)
Quadrupole (002)	2.5	8	Bertrand (1981)
Monopole (000)	3		Youngblood, et al., (1981)
Giant Octupole	5	10	Carey, et al., (1980) Morsch, et al., (1980) Yamagata, et al., (1981)
Gamow-Teller (110)	4		Horen, et al., (1980) Bainum, et al., (1980)

Table III. Particle-hole interference in the vibration self-energy. The sign of the quantity (45) is shown for all possible values of the quantum numbers associated with the initial vibration and with the intermediate doorway vibration. Note that if either vibration is purely scalar, the interference is destructive.

n_0, σ_0 \ n_r, n_r'	00	10	01	11
00	-	-	-	-
10	-	+	-	+
01	-	-	+	+
11	-	+	+	-

Appendix A. Evaluation of Strength Functions in Doorway Approximations

The strength function we wish to evaluate is defined by eq. (1). It is useful to express this formally in terms of the resolvent of the Hamiltonian,

$$S(E) = \frac{1}{\pi} \mathrm{Im}\langle o|Q(H-E-i\eta)^{-1}Q|o\rangle \tag{A1}$$

We next define the state $|a\rangle$ that is produced from the ground state by the operator,

$$|a\rangle = \frac{Q|o\rangle}{\sqrt{\langle o|QQ|o\rangle}} \tag{A2}$$

and separate the Hamiltonian into parts that act on a and the rest

$$H = E_a|a\rangle\langle a| + \sum_\alpha \left[V_{a\alpha}(|a\rangle\langle\alpha| + |\alpha\rangle\langle a|) + E_\alpha|\alpha\rangle\langle\alpha|\right] + H' \tag{A3}$$

The states $|\alpha\rangle$ with $V_{a\alpha} \neq 0$ are the doorways. If H' is neglected, the resolvent can be evaluated algebraically as [1]

$$S(E) = \langle o|QQ|o\rangle \frac{1}{\pi} \mathrm{Im}\left(\frac{1}{E_a - E - \sum_\alpha \frac{V_{\alpha a}^2}{E_\alpha - E} - i\eta}\right) \tag{A4}$$

We next average this strength function over energy with a weight function

$$\rho(E-E') = \frac{1}{\pi} \frac{I}{(E-E')^2 + I^2} \tag{A5}$$

As noted by Brown, et al., (1959), averaging with this weight is

(1) This was first exploited by Feshbach, (1958), for scattering problems.

equivalent to evaluating S at an energy E + iI,

$$\bar{S}(E) = \int S(E')\rho(E-E')dE' = S(E+iI) \tag{A6}$$

$$= \frac{\langle o|QQ|o\rangle}{\pi} \mathrm{Im} \frac{1}{E_a - E - iI - \sum_\alpha V_{a\alpha}^2/(E_\alpha - E - iI)} \tag{A7}$$

We can then express the averaged strength function in a form that resembles the Breit-Wigner distribution, except that the width is energy-dependent: [2]

$$\bar{S}(E) = \frac{1}{\pi} \frac{\Gamma(E)/2 + I}{(E_a - E - \mathrm{Re}\Sigma(E))^2 + (\Gamma(E)/2 + I)^2} \tag{A8}$$

where

$$\mathrm{Re}\Sigma(E) = \sum_\alpha \frac{V_{\alpha a}^2 (E_\alpha - E)}{(E_\alpha - E)^2 + I^2} \tag{A9}$$

$$\Gamma(E) = \sum_\alpha \frac{V_{\alpha a}^2 I}{(E_\alpha - E)^2 + I^2} \tag{A10}$$

Eq. (A8) is exact for the truncated Hamiltonian, but is useful only if Σ varies slowly with energy. It remains to be seen for each case whether this occurs for averaging intervals I that are not too large.

In calculating the strength function for vibrations, the RPA response is first evaluated. This may be distributed over a number of states, if Landau damping is present. It is then necessary to generalize eq. (A7) by replacing the single vector a by the subspace of RPA states. Eq. (A7) is still correct as a matrix

(2) The derivation may also be found in Bohr and Mottelson, (1969), p. 306.

eration,

$$\bar{S}(E) = \frac{1}{\pi} \mathrm{Im} \langle o|\mathcal{O}\left(H_p - E - i\Gamma - \sum_\alpha \frac{V_{p\alpha} V_{\alpha p}}{E_\alpha - E - i\Gamma}\right)^{-1} \mathcal{O}|o\rangle \qquad (A11)$$

Here H_p is the Hamiltonian matrix in the RPA space, and $V_{p\alpha} V_{\alpha p}$ is a dyadic in this space. Soloviev, et al., (1977) carry out the matrix inversion of eq. (A9) by Cramer's rule

$$\bar{S}(E) = \frac{1}{\pi} \mathrm{Im} \sum_{a,a'} \frac{\langle o|\mathcal{O}|a\rangle M_{aa'} \langle a'|\mathcal{O}|o\rangle}{\mathrm{Det}\left|H_p - E - i\Gamma - \sum_\alpha \frac{V_{p\alpha} V_{\alpha p}}{E_\alpha - E - i\Gamma}\right|} \qquad (A12)$$

where a,a' are states in the particle-hole space, and $M_{aa'}$ is the minor of the determinant in the denominator of eq. (A12).

Appendix B. Doorway Coupling for Particle-hole Vibrations

We present here the formulas for vibrational self-energies associated with doorways made from particle-hole + vibration states. The particle and hole states are labeled by $k = (j_k t)$ and $i = (j_i t)$ respectively, where j is the angular momentum and $t = \frac{1}{2}$ is the isospin. The vibrations are labeled by the quantum numbers $\alpha = (n\lambda\tau)$ where τ(=0 or 1) specifies the isospin of the mode, and λ is the angular momentum. Because more than one mode of a given $\lambda\tau$ may exist, an index n is added to completely specify the state. The important quantities in the particle-vibration description are the coupling matrix elements, $M(j,j';\alpha)$ giving the reduced matrix elements of the residual interaction between particles and vibrations. The $M(j,j';\alpha)$ is calculated via a single particle field $F_{\lambda\tau}$ as

$$M(jj';\alpha) = \langle j|||F_{\lambda\tau}|||j'\rangle \Lambda_\alpha \qquad (B1)$$

where Λ_α is a normalization constant to be specified below. We saw in eq. (24) that a suitable field for coupling to collective ($\tau = 0$) states is the derivative of the central potential. In this surface coupling model $F_{L0} = R \frac{dU_0}{dr} Y_L$ and $M(jj';\alpha)$ is given by

$$\Lambda(\alpha)\langle j|||R \frac{dU_0}{dr} Y_L|||j'\rangle = \frac{\beta_{L,(\alpha')}}{\sqrt{2L+1}} \langle j|R \frac{dU_0}{dr}|j'\rangle\langle j||Y_L||j'\rangle\langle t||1||t\rangle \qquad (B2)$$

The reduced matrix element of the spherical harmonic Y_L is given by

$$\langle j_\gamma||Y_L||j_\alpha\rangle = (-)^{j_\alpha+L-j_\gamma} \sqrt{\frac{(2L+1)(2j_\alpha+1)}{4\pi}} \langle j_\alpha \tfrac{1}{2} L0|j_\gamma \tfrac{1}{2}\rangle \text{ if } \ell_\alpha - \ell_\gamma + L \text{ is even}$$
$$= 0 \text{ if } \ell_\alpha - \ell_\gamma + L \text{ is odd} \qquad (B3)$$

and the reduced matrix element of the unit operator in isospin is

$$\langle \tfrac{1}{2} \| 1 \| \tfrac{1}{2} \rangle = \sqrt{2} \tag{B4}$$

The matrix element $M(jj';\alpha)$ has the following symmetry under interchange of j and j',

$$M(jj';\alpha) = -c(F_{\lambda\tau})(-)^{j'+j-\lambda+1-\tau} M(j'j;\alpha) \tag{B5}$$

where $c(F_{\lambda\tau}) = \pm 1$ relates the particle matrix element of $F_{\lambda\tau}$ to the corresponding hole matrix element.†

The RPA amplitudes for a particle-hole configuration in a vibration can be calculated in terms of the single-particle energies ϵ_j, the vibrational energy E_α, and the reduced coupling matrix elements $M(ki;\alpha)$ as

$$\left.\begin{matrix} X(ki,\alpha) \\ Y(ki,\alpha) \end{matrix}\right\} = \frac{1}{\sqrt{2(2\lambda_\alpha+1)}} \frac{M(ki,\alpha)}{(\epsilon_k - \epsilon_i \mp E_\alpha)} \tag{B6}$$

Here X is the usual amplitude to create the vibration with the (ki) particle-hole operators, and Y is the amplitude to create the vibration by annihilating the (ki) configuration. The normalization constant A_α in (B1) is such that the X,Y amplitudes have the normalization

$$\sum_{ki} (X^2(ki,\alpha) - Y^2(ki,\alpha)) = 1 \tag{B7}$$

We now write the contributions to the self energy of a vibration α, associated with the perturbation graphs a) and b) in Fig. 26,

$$\Sigma_{a)} = \sum_{\substack{\alpha' \\ ki,k'}} X^2(ki;\alpha) \frac{M^2(k'k;\alpha')}{E-(\epsilon_{k'}-\epsilon_i+E_{\alpha'})} \left[\frac{1}{2(2j_k+1)}\right] \tag{B8}$$

and

$$\Sigma_{b)} = \sum_{\substack{\alpha' \\ ki;k'i'}} X(ki;\alpha)X(k'i';\alpha) \frac{M(k'k;\alpha')M(ii';\alpha')}{E-(\epsilon_{k'}-\epsilon_i+E_{\alpha'})} [c(F_{\alpha'})R_{\lambda'}R_{\tau'}] \tag{B9}$$

The remaining two graphs in Fig. 22 may be obtained by interchanging particle and hole labels in (B8,B9). The quantities R are the recoupling coefficients for the angular momentum and isospin. They are given by

$$R_{\lambda'} = (-)^{j_k+j_i+\lambda} \begin{Bmatrix} j_k & j_i & \lambda \\ j_i & j_k & \lambda' \end{Bmatrix} \tag{B10}$$

$$R_\tau = (-)^{\tau+1} \begin{Bmatrix} \tfrac{1}{2} & \tfrac{1}{2} & \tau \\ \tfrac{1}{2} & \tfrac{1}{2} & \tau' \end{Bmatrix} \tag{B11}$$

While (B8-11) are quite straightforward, the numerous summations makes these formulas somewhat tedious to evaluate. There are two tricks which can simplify the work. In the RPA theory based on the surface coupling, the expression

$$\sum_{\alpha'} \frac{M(kk';\alpha')M(k''k''',\alpha')}{E - E_{\alpha'}} \tag{B12}$$

is proportional to the RPA response function for the operator $F_{\lambda\tau}$. The RPA response function can be evaluated in terms of the independent particle response, without the need to explicitly construct the RPA eigenstates α' (Bertsch, et al., 1979).

† For the density operator $c = -1$; for other cases, see Bohr and Mottelson (1969), p. 313 and app. 3B.

Another simplification eliminates the need for the double summation of (ki) and (ki'i) in eq. (B9). This is accomplished by adding the particle amplitude to the hole amplitude before squaring, as depicted in the top line of Fig. 22. Using the angular momentum coupling scheme $((\lambda' j_{k'}) j_k j_i)_\lambda$ for the doorway state, the matrix element for the combined amplitude is

$$V_{\lambda,(k'\alpha'i)} = \sum_k \left(\frac{X(ki,\alpha)M(k'k;\alpha')}{\sqrt{2(2j_k+1)}} + \sum_{i'} \frac{X(k'i',\alpha)M(ii';\alpha)}{\sqrt{2(2j_{i'}+1)}} S_\tau S_{\lambda'} c(F_{\alpha'}) \right) \quad \text{(B13)}$$

The recoupling coefficients S in eq. (B13) is given by

$$S_{\lambda'} = (-)^{j_k+j_i+\lambda} \sqrt{(2j_k+1)(2j_{i'}+1)} \begin{Bmatrix} j_k & j_i & \lambda \\ j_{i'} & j_{k'} & \lambda' \end{Bmatrix} \quad \text{(B14)}$$

and similarly for the τ recoupling. The self-energy is then evaluated as

$$\Sigma = \sum_{\alpha' k' i} \frac{V^2_{\lambda,(k'\alpha'i)}}{E-(\varepsilon_{k'}-\varepsilon_i+E_{\alpha'})} \quad \text{(B15)}$$

The strength functions and widths may be evaluated from the self energy (B15) as in eq. (A8-10).

All time orderings of the intermediate vertices in the graphs of Fig. 22 need to be included in a consistent second-order calculation of the self-energy. With the (ki) and (k'i') sums restricted to particle-hole states, eqs. (B8,9) only have the time orderings of Fig. 26(a),(b), lacking amplitudes such as Fig. 26(c). Fortunately, the damping calculation only requires the residue of the poles in Σ at $E = \varepsilon_{k'} - \varepsilon_i - E_{\alpha'}$, and these residues are given correctly by (B8,9) if the sum over indices k,i' ranges independently over particles and holes.

We also give the formulas for the self energy in LS coupling, as the coherence properties are more evident in this coupling scheme. The particle states are then labeled by orbital angular momentum ℓ, the fields have an additional σ-dependence, $F = F_{\lambda\sigma}$, and a σ-reduced matrix element will be present in $M(jj',\alpha)$. The bracketed expressions in (B8), (B9) are then changed to the following

$$\left[\frac{1}{2(2j_k+1)}\right] \to \left[\frac{1}{4(2\ell_k+1)}\right] \quad \text{(B16)}$$

$$\left[c(F_{\alpha'})R_{\lambda'}R_\tau\right] \to \left[c(F_{\alpha'})R_{\lambda'}R_\sigma R_\tau\right] \quad \text{(B17)}$$

The new $R_{\lambda'}$ is the same as (B10) with j labels changed to ℓ labels. The R_σ is the same as (B11) for R_τ with the τ label changed to σ.

Appendix C. Damping in Fermi Liquid Theory

We examine here the damping of collective vibrations in Fermi liquid theory, with a view toward macroscopic treatments of the damping using notions such as viscosity. In the Landau theory, there are two types of damping: the Landau damping associated with single-particle motion, discussed in Sec. IVB, and the collisional damping. For fixed temperature, the collisional damping gives rise to viscosity in the limit in which the frequency of the excitation energy is small compared to the particle collision frequency. At zero temperature, the collisional damping may be directly compared with the perturbation treatment of damping in App. B. However, first the relation between Landau's distribution function $n_p(r,t)$ and the quantum amplitudes must be explained. We consider an infinite medium with particle-hole excitations carrying momentum q. We can define the amplitude for a particle-hole state in the vibration, $\langle vib|a^\dagger_{\vec{p}+\vec{q}}a_{\vec{p}}|0\rangle$. In the conventional notation of RPA, this is either the amplitude $X_{\vec{p}+\vec{q},\vec{p}}$ or $Y_{\vec{p},\vec{p}+\vec{q}}$ depending on whether p+q is the particle state and p the hole state, or vice versa.

The distribution function δn of Landau theory is related to these amplitudes by summing over configurations with a given angle θ_p between $\vec{p}$ and $\vec{q}$ (cf. e.g. Brown, 1972):

$$\delta n(\theta_p) = \int \langle vib|a^\dagger_{\vec{p}+\vec{q}}a_{\vec{p}}|0\rangle \frac{p^2dp}{(2\pi)^3} = \frac{p_F^2 q\cos\theta_p}{(2\pi)^3} \cdot \begin{cases} X_{\vec{p}+\vec{q},\vec{p}} & \theta_p < \frac{\pi}{2} \\ -Y_{\vec{p},\vec{p}+\vec{q}} & \theta_p > \frac{\pi}{2} \end{cases} \quad (C1)$$

We first verify that the solution of the collisionless Boltzmann

equation for $\delta n(\theta_p)$ is equivalent to eq. (B6) for X,Y. The Boltzmann equation is

$$\frac{\partial n}{\partial t} + \frac{\vec{p}}{m^*}\cdot\vec{\nabla}_r n - \vec{\nabla}_r U\cdot\vec{\nabla}_p n = I \quad (C2)$$

with $$U_p(\vec{r},t) = \int f(\vec{p},\vec{p}')n_{\vec{p}'}(\vec{r},t)\frac{d^3p'}{(2\pi)^3}$$

and I the collison integral. Landau's solution is obtained by dropping the collision integral, and linearizing in the time-varying parts of n and U. The $\delta n_{\vec{p}}$ is peaked on the Fermi surface and in the limit of $q \ll p_F$, the dependence of $\delta n_{\vec{p}}$ on $|p|$ can be neglected. Then the amplitude only depends on the angle θ_p, and the equation for excitations of frequency ω is

$$\delta n(\theta_p) = \frac{q\cos\theta_p}{-\omega + \frac{pq}{m^*}\cos\theta_p}\int \frac{\delta U(\theta_p)}{\delta n(\theta_{p'})}\,\delta n(\theta_{p'})\,d\cos\theta_{p'} \quad (C3)$$

where $$\delta n(\theta_p) = p_F^2 q\cos\theta_p\,\delta n_{\vec{p}}(r,t)\ , \qquad |\vec{p}| = p_F\ .$$

To compare with (C1), note that the number of particle-hole pairs in (C1) for $q\to 0$ is proportional to $\int(1-n_{\vec{p}+\vec{q}})n_{\vec{p}}dp = q\cos\theta\,\delta(p-p_p)$. The denominator in (C3) is just the $q\to 0$ limit of the energy denominator of (B6),

$$\frac{1}{-\omega + \frac{pq}{m^*}\cos\theta} = \frac{1}{-E + (\epsilon_{particle} - \epsilon_{hole})} \quad (C4)$$

The change in sign of the numerator when $\theta_p > \frac{\pi}{2}$, together with the relabeling of particle and hole states when $\theta_p > \frac{\pi}{2}$, gives rise to the sign change in E on the Y amplitude in eq. (B6). Finally, the integral over the potential $\frac{\delta U}{\delta n}$ is just the matrix element of

the potential field exciting a particle-hole configuration, equivalent to M in eq. (B6).

We can now analyze the collision integral in the linear approximation and show that it is equivalent to the perturbation result,[1] (B8-10). Assuming that the distribution function has an additional time dependence $e^{-\Gamma^{\downarrow}t/2}$, eq. (C2) with the collision integral gives

$$\frac{\Gamma}{2}\,\delta n(\theta_p) = \int d\cos\theta_{p'}\,\frac{\delta I(\theta_p)}{\delta n(\theta_{p'})}\,\delta n(\theta_{p'}), \qquad \text{(C5)}$$

where we have formally evaluated the collision integral in the linear approximation. Landau (1957) writes the collision integral for the damping of a collective state as

$$I(\vec{p}) = \int \frac{d^3\vec{p}_2 d^3\vec{p}_3 d^3\vec{p}_4}{(2\pi)^9}\,\pi\,|v(\vec{p}+\vec{p}_2\leftrightarrow\vec{p}_3+\vec{p}_4)|^2\delta(\varepsilon_{\vec{p}_3}+\varepsilon_{\vec{p}_4}+\omega-\varepsilon_{\vec{p}_2}-\varepsilon_{\vec{p}}) \qquad \text{(C6)}$$

$$\times\delta^3(\vec{p}_3+\vec{p}_4-\vec{p}_2-\vec{p})\left[n_{\vec{p}}n_{\vec{p}_2}(1-n_{\vec{p}_3})(1-n_{\vec{p}_4})-(1-n_{\vec{p}})(1-n_{\vec{p}_2})n_{\vec{p}_3}n_{\vec{p}_4}\right]$$

This differs from the Uehling-Uhlenbeck form[2] of the collision integral by the presence of the vibrational frequency ω in the energy-conserving δ-function. In a model with doorways based on particle-hole + vibration states rather than 2p-2h states, the collision integral would be

$$I(p) = \int \frac{d^3p_2}{(2\pi)^3}\,\pi\sum_\alpha|v(\vec{p}\leftrightarrow\vec{p}_\alpha+\vec{p}')|^2\delta(\varepsilon_{\vec{p}'}+\omega+E_{\vec{p}_\alpha}-\varepsilon_{\vec{p}})\times \qquad \text{(C7)}$$

$$\delta^3(\vec{p}'+\vec{p}_\alpha-\vec{p})\left[n_{\vec{p}}(1-n_{\vec{p}'})-(1-n_{\vec{p}})n_{\vec{p}'}\right]$$

We will analyze (C7) rather than (C6) for simplicity and to make a

[1] The equivalence has also been demonstrated by K. Ando and G. Holzwarth (1982).

[2] See (Uehling and Uhlenbeck, 1935). Derivations of the collision integral may be found in Abriksov, et al., (1963), Kadanoff and Baym (1962) and Wölfle (1970).

parallel with the treatment in App. B. The distribution function n appears in four places in I, so there will be four terms in $\frac{\delta I}{\delta n}$. Each of these terms may be associated with the imaginary part of one of the perturbation graphs of Fig. 22. To make the correspondence, draw a particle line k for a factor of $(1-n_k)$ and a hole line k for a factor $n^0(k)$, where k = p or p'. The incoming vibration, $\delta n(k)$, connects to fermion lines k+q,k. The outgoing fermion lines are p+q,p, since the graph is a contribution to $\delta n(p)$. The requirement that the intermediate state have the vibration produced together with the fermion p or p+q determines how the outer fermion lines are connected to the intermediate vibration. The lines not part of the doorway state can be either particle or holes, depending on $|k|-p_F$, and we will draw these as horizontal lines. The four graphs from the four terms in (C7) are shown in Fig. 27.

The only tricky point in making the identification is the fact that (B8-9) is based on only X-type amplitudes, while δn identifies with both X and Y amplitudes. The $\delta n(p')$ identifies with a Y amplitude when p' is in the backward hemisphere, $\theta_{p'} > \frac{\pi}{2}$. However, we have generalized the definition of the X amplitudes to include time orderings such as 26(c), which involve orbitals in the backward hemisphere. In fact, the contribution from $\theta_{p'} > \frac{\pi}{2}$ in eq. (C5) is algebraically identical to the perturbative contribution from Fig. 26(c), in the $q \to 0$ limit. Thus the linearized collision integral is completely equivalent to the perturbation treatment.

We now compare the collisional damping with macroscopic theories of damping based on fluid equations. Auerbach and

Yeverechyahu (1975) assume that the vibrations can be described by equations in which the velocity field of particles is subject to dissipative forces given by

$$\left.\frac{\partial \vec{v}_\tau}{\partial t}\right|_{\text{dissipative}} = +\nu(\nabla^2\vec{v}_\tau + \frac{1}{3}\nabla\nabla\cdot\vec{v}_\tau) - \gamma(\vec{v}_\tau - \vec{v}_{-\tau}) \qquad \text{(C8)}$$

Here the τ label distinguishes neutrons and protons. The ν and γ are intended to be constants, independent of nuclear size or type of vibration. In the microscopic approach, we expand $\delta n(p)$ in multipoles of $\cos\theta_p$, with $L = 0$ associated with particle density, and $L = 1$ with current. The $L = 0$ moment is unaffected by the collision integral, due to conservation of particle number. The $L = 1$ moment of density vibrations, proportional to the nucleon current, is unaffected by the collision integral due to current conservation. The collision integral can damp the $L = 1$ moment of isovector vibrations, as assumed in the last term in eq. (C8). However, evaluation of the collision integral will give a damping rate proportional to ω^2 for (C6), and also for (C7) if the density of doorway vibrations increases linearly with E_α. Thus a constant γ in (C8) is unjustified. The next multipole is $L = 2$, the distortion of the Fermi surface, which is always subject to damping. Again the collision integral would give a damping proportional to ω^2, and proportional to the amount of $L = 2$ Fermi surface distortion in the vibrational state. The amount of $L = 2$ distortion of the Fermi surface can be estimated from the second order term in the expansion of $\delta n(\theta)$ in the large-ω limit,

$$\delta n(\theta) \sim \frac{q\cos\theta}{\omega - \frac{pq}{m^*}\cos\theta} \sim \frac{q\cos\theta}{\omega}\left(1 + \frac{pq\cos\theta}{\omega m^*} + \left(\frac{pq}{m^*\omega}\cos\theta\right)^2 + \ldots\right.$$

We see the relative amount of $L = 2$ is of order $\sim\left(\frac{pq}{\omega m^*}\right)^2$. Thus the damping rate can also be seen to scale with q as

$$\Gamma \sim \omega^2\left(\frac{pq}{\omega m^*}\right)^2 \sim q^2.$$

This q^2 dependence then justifies the first term in (C8), which has a constant multiplying the second space derivative of a macroscopic field. However, it should be apparent from the derivation, that the macroscopic treatment has no more than a qualitative validity for the nuclear vibrations.

References

Abrikosov, A., L. Gorkov and I. Dzyaloshinski, 1963, Methods of Quantum Field Theory in Statistical Physics, Pergamon, Chap. 40.

Adachi, S., and S. Yoshida, 1978, Nucl. Phys. A306, 53.

Agrawal, D. C., and P. C. Sood, 1975, Phys. Rev. C 11, 1854.

Anantaraman, N., G. M. Crawley, A. Galonsky, C. Djalali, N. Marty, M. Morlet, A. Willis, and J. C. Jourdain, 1981, Phys. Rev. Lett. 46, 1318.

Ando, K., and G. Holzwarth, 1982, private communication.

Auerbach, N., and A. Yeverechyahu, 1975, Ann. Phys. 95, 35.

Bainum, D.E., J. Rapaport, C.D. Goodman, D.J. Horen, C.C. Foster, M.B. Greenfield, and C.A. Goulding, 1980, Phys. Rev. Letters 44, 1751.

Berman, B. L., and S. C. Fultz, 1975, Rev. Mod. Phys. 47, 713.

Bernard, V., and N. Van Giai, 1979, Nucl. Phys. A327, 397.

Bertrand, F. E., 1981, Nucl. Phys. A354, 129.

Bertrand, F. E., K. van der Borg, A. G. Drentje, M. N. Harakeh, A. van der Plicht, and A. van der Woude, 1978, Phys. Rev. Lett. 40, 635.

Bertrand, F. E., G. R. Satchler, D. J. Horen, J. R. Wu, A. D. Bacher, G. T. Emery, W. P. Jones, D. W. Miller, and A. Van der Woude, 1980, Phys. Rev. C22, 1832.

Bertsch, G., 1971, Phys. Letters 37B, 470.

Bertsch, G., P. F. Bortignon, R. A. Broglia and C. H. Dasso, 1979, Phys. Lett. 80B, 161.

Bertsch, G., and I. Hamamoto, Phys. Rev. C26 (1982) to be published.

Bertsch, G., and Tsai, S. F., 1975, Phys. Reports 18C 125.

Bethe, H. A., and J. S. Levinger, 1950, Phys. Rev. 78 115.

Bohr, A., 1952, Mat. Fys. Medd. Dan. Vid. Selsk. 26, No.14.

Bohr, N., 1936, Nature 137, 344.

Bohr, A., and B. Mottelson, 1969, Nuclear Structure, Vol. I, Benjamin.

Bohr, A., and B. Mottelson, 1975, Nuclear Structure, Vol. II, Benjamin.

Bortignon, P.F., R. A. Broglia, and F. Zardi, 1982, Conference on Spin Excitations in Nuclei, Telluride, to be published.

Bortignon, P., and R. Broglia, 1981a, Phys. Lett. 102B, 303.

Bortignon, P., and R. Broglia, 1981b, Nucl. Phys. A371, 405.

Bouyssy, A., H. Ngo, and N. Vinh Mau, 1981, Nucl. Phys. A371, 173.

Brieva, F. A., and J. R. Rook, 1977, Nucl. Phys. A291, 299.

Broglia, R. A., V. Paar and D.R. Bes, 1971, Phys. Lett. 37B, 159.

Broglia, R. A., and A. Winther, 1981, Heavy Ion Reactions, Benjamin, 246.

Brown, G. E., Many-Body Problems, 1972, North-Holland, eq. 25.16.

Brown, G., C. de Dominicis, and J. Langer, 1959, Ann. Phys. 6, 209.

Brown, G., and M. Rho, 1981, Nuclear Physics A372, 397.

Brueckner, K.A., R.J. Eden, and N.C. Francis, 1955, Phys. Rev. 100, 891.

Buenerd, M., and D. Lensbrun, 1981, Phys. Rev. C24, 1356.

Carey, T.A., W.D. Cornelius, N.J. DiGiacomo, J.M. Moss, G.S. Adams, J.B. McClelland, G. Pauletta, C. Whitten, M. Gazzaly, N. Hintz, and C. Glasshausser, 1980, Phys. Rev. Lett. 45, 239.

Coulter, P.W., and G.R. Satchler, 1977, nucl. Phys. A293, 269.

Dambasuren, D., V. G. Soloviev, C. Stoyanov, and A. I. Vdovin, 1976, Journal of Physics G 2, 25.

Danos, M., and W. Greiner, 1965, Phys. Rev. 138B, 876.

Dehesa, J. S., S. Krewald, J. Speth and A. Faessler, 1977, Phys. Rev. C15, 1858.

Djalali, C., N. Marti, M. Morlet, and A. Willis, 1982, Nucl. Phys. A380, 42.

Dover, C. B., R. H. Lemmer, and F. J. W. Hahne, 1972, Ann. Phys. 70, 458.

Dowell, D. H., L. S. Cardman, P. Axel, G. Bolme and S.E. Williamson, 1982, Phys. Rev. Lett. 49, 113.

Dubois, D.F., 1959, Ann. Phys. 8, 24.

Edmonds, A. R., Angular Momentum in Quantum Mechanics,

1960, Princeton University Press.

Erskine, J. R., A. Marinov, and J. P. Schiffer, 1966, Phys. Rev. 142, 633.

Fantoni, S., B. L. Friman, and V. R. Pandharipande, 1981, Phys. Lett. 104B, 89.

Feshbach, H., 1958, Ann. Phys. 5, 357.

Feshbach, H., C. E. Porter, and V. F. Weisskopf, 1954, Phys. Rev. 96, 448.

Fiebig, H. R., and J. Wambach, 1982, Nucl. Phys. in press.

French, J.B., P.A. Mello and A. Pandey, 1978, Ann. Phys. 113, 277.

Gaarde, C., J. S. Larsen, M. N. Harakeh, S. Y. van der Werf, M. Igarashi, and A. Mueller-Arnke, 1980, Nucl. Phys. A334, 248.

Gaarde, C., J. Rapaport, T. N. Taddeucci, C. D. Goodman, C. C. Foster, D. E. Bainum, C. A. Goulding, M. B. Greenfield, D. J. Horen, and E. Sugarbaker, 1981, Nucl. Phys. A369, 258.

Gales, S., G. M. Crawley, D. Weber, and B. Zwieglinski, 1978, Phys. Rev. C 18, 2475.

Gales, S., C.P. Massolo, S. Fortier, E.Gerlic, J. Guillot, E. Hourani, J.M. Maison, J.P. Schapiro, B. Zwieglinksi, P. Martin, and V. Comparat, 1982a, Phys. Rev. Lett. 48, 1593.

Gales, S., G. M. Crawley, D. Weber and B. Zwieglinski, 1982b, Nucl. Phys. A381, 173.

Galitskii, V. M., 1958, Sov. Phys. JETP 7, 104.

Gerlic, E., G. Berrier-Ronsin, G. Duhamel, S. Gales, E. Hourani, H. Langevin-Joliot, M. Vergnes, and J. Van de Wiele, 1980, Phys. Rev. C21, 124.

Horen, D. J., C. D. goodman, C. C. Foster, C. A. Goulding, M. B. Greenfield, J. Rapaport, D. E. Bainum, E. Sugarbaker, T. G. Masterson, F. Petrovich, W. G. Love, 1980, Phys. Lett. 95B, 27.

Hoshino, T., and A. Arima, 1976, Phys. Rev. Letters 37, 266.

Jacob, G., and T. A. J. Maris, 1973, Rev. Mod. Phys. 45, 6.

Jeukenne, J. P., A. Lejeune, and C. Mahaux, 1977, Phys. Rev. C16, 80.

Jeukenne, J. P., A. Lejeune, and C. Mahaux, 1976, Phys. Reports 25C, 83.

Kadanoff, L. and G. Baym, 1962, Quantum Statistical Mechanics, Benjamin.

Knüpfer, W., and M. G. Huber, 1976, Z. Physik A276, 99.

Koeling, T., and F. Iachello, 1978, Nucl. Phys. a295, 45.

Knöpfle, K.T., G.J. Wagner, P. Paul, H. Breuer, C. Mayer-Boriche, M. Rogge, and P. Turek, 1978, Phys. Lett. 74B, 191.

Krotschek, E., R. A. Smith, and A. D. Jackson, 1981, Phys. Lett. 104B, 421.

Kuchnir, F. T.., P. Axel, L. Criegee, D. M. Drake, A. O. Hanson, and D. C. Sutton, 1967, Phys. Rev. 161, 1230.

Kühner, G., D. Meuer, S. Muller, A. Richter, E. Spamer, O. Titze, and W. Knupfer, 1981, Phys. Lett. 104B, 189.

Landau, L., 1958, Soviet Physics JETP 5, 101.

Lane, A. M., R. G. Thomas, and E. P. Wigner, 1955, Phys. Rev. 98, 693.

Lee, T. H., and S. Pittel, 1975, Phys. Rev. C11, 607.

Lev, A., W. Beres and M. Divadeenam, 1973, Phys. Rev. Lett. 31, 555.

Liu, K. F., and G. E. Brown, 1976, Nucl. Phys. A265, 385.

Mahaux, C., and H. Ngo, 1981, Phys. Lett. 100B, 285.

Morsch, H.P., M. Rogge, P. Turek, and C. Mayer-Boricke, 1980, Phys. Rev. Lett. 45, 337.

Mottelson, B., 1960, Proc. of the International School of Physics "E. Fermi", Course XV, Ed. G. Racah, Academic, p. 44.

Mougey, J., M Bernheim, A. Bussiere, A. Gillebert, P. X. Ho, M. Priou, D. Royer, I. Sick, and G.J. Wagner, 1976, Nucl. Phys. A262, 461.

Mughabghab, S. F., and D. I. Garber, 1973, Neutron Cross Sections, Vol. I, BNL 325.

Nakamura, K., S. Hiramatsu, T. Kamae, H. Muramatsu, N. Izutsu, and Y. Watase, 1974, Phys. Rev. Lett. 33, 853.

Negele, J. W., and K. Yazaki, 1981, Phys. Rev. Lett. 47, 71.

Nix, J.R., and A.J. Sierk, 1980, Phys. Rev. C21, 396.

O'Dwyer, J. F., M. Kawai, and G. E. Brown, 1972, Phys. Lett. 41B, 259.

Okada, K., H. Ejiri, T. Shibata, Y. Nagai, T. Motobayashi, H. Ohsumi, M. Noumachi, A. Shimizu, K. Maeda, 1982, Phys. Rev. Lett. 48, 1382.

Orland, H., and R. Schaeffer, 1978, Nucl. Phys. A299, 442.

Osterfeld, F., 1982, Phys. Rev. C26, 762.

Osterfeld, F., J. Wambach, and V.A. Madsen, 1981, Phys. Rev. C23, 179.

Pines, D., and P. Nozieres, 1966, Theory of Quantum Liquids, Benjamin, 117.

Ponomarev, V., V. Soloviev, C. Stoyanov, and A. Vdovin, 1979, Nucl.Phys. A323, 446.

Rao, C. L., M. Reeves and G. R. Satchler, 1973, Nucl. Phys. A207, 182.

Rapaport, J., V. Kulkarni, and R. W. Finlay, 1979, Nucl. Phys. A330, 15.

Ring, P., and J. Speth, 1974, Nucl. Phys. A235, 315.

Satchler, G. R., 1972, Nucl. Phys. A195, 1.

Siemssen, R., W. Jones, W. Jacobs, C. Foster, D. Miller, M. Saber and F. Soga, 1981, Phys. Lett. 103B, 323.

Shakin, C., 1963, Ann. Phys. 22, 373.

Shlomo, S., and G. Bertsch, 1975, Nucl. Phys. A243, 507.

Skwiersky, B. M., C. M. Baglin, and P. D. Parker, 1974, Phys. Rev. C 9, 910.

Soloviev, V. G., Ch. Stoyanov and A. I. Vdovin, 1977, Nucl. Phys. A288, 376.

Soloviev, V. G., Ch. Stoyanov and A. I. Vdovin, 1980, Nucl. Phys. A342, 261.

Speth, J., and A. van der Woude, 1981, Reports in Progress in Physics, 44, 261.

Steffen, W., H.-D. Graf, W. Gross, D. Meuer, A. Richter, E. Spamer, O. Titze, and W. Knupfer, 1980, Phys. Lett. 95B, 23.

Stuirbrink, A., G. Wagner, K. Knopfle, L. Pao, G. Mairle, H. Riedesel, and K. Schindler, 1980, Z. Physik A297, 307.

Stroher, H., R. Fischer, J. Drexler, K. Huber, U. Kneissl, R. Patzek, H. Ries, and W. Wilke, 1981, Phys. Rev. Lett. 47, 318.

Uehling, E. A., and G. E. Uhlenbeck, 1933, Phys. Rev. 43, 552.

Ui, H., 1975, Proc. Conf. on New Giant Resonances, Sendai, 105.

Van Giai, N., and H. Sagawa, 1981, Nucl. Phys. A371, 1.

Wambach, J., V. Mishra, and C. H. Li, 1982, Nucl. Phys. A380, 285.

Wölfle, P., 1970, Z. Physik 232, 30.

Yamagata, T., S. Kishimoto, K. Yuasa, K. Iwamoto, B. Saeki, M. Tanaka, T. Fukuda, I. Miura, M. Inoue, and H. Ogata, 1981, Phys. Rev. C23, 937.

Youngblood, D., C. Rozsa, J. Moss, D. Brown, and J. Bronson, 1977, Phys. Rev. Lett. 39, 1188.

Youngblood, D.H., P. Bogucki, J.D. Bronson, U. Garg, Y.-W. Lui, and C.M. Rozsa, 1981, Phys. Rev. C23, 1997.

FIGURE CAPTIONS

Fig. 1 - Spectroscopy of ^{43}Sc from the ^{40}Ca(^{3}He,d)^{43}Sc reaction, measured by Erskine, Marinov and Schiffer (1966). The ground state has practically all of the $f_{7/2}$ strength, while for higher orbits the strength is spread over several states.

Fig. 2 - The energy spectrum of ^{3}He in the proton pickup reaction, ^{90}Zr(d,^{3}He)^{89}Y, from Stuirbrink, et al. (1980). The shaded bump shows an angular dependence and analyzing power characteristic of the $f_{7/2}$ hole orbit.

Fig. 3 - The energy spectrum of tritons particles from the reaction ^{116}Sn(d,t)^{115}Sn (Siemssen, et al., 1981).

Fig. 4 - The s-wave neutron strength function (Mughabghab and Garber, 1973). The strength function S_0 is plotted in the standard units, eq.(2). Solid and dashed lines show the optical model fit, eq. (4).

Fig. 5 - The p-wave neutron strength function S_1, as in Fig. 4.

Fig. 6 - Phase shift analysis of elastic proton scattering on ^{16}O, from Skwiersky, et al., (1974). In a) is shown the phase shift in degrees. In b) is shown the reflection coefficient η for the $\ell = 3$ partial wave.

Fig. 7 - The photoneutron cross section for ^{4}He, from Berman and Fultz (1975).

Figure Captions (continued)

Fig. 8 - The photoneutron cross section for ^{208}Pb, from Berman and Fultz (1975).

Fig. 9 - Systematics of the width of the giant dipole state, from Berman and Fultz (1975). Only spherical nuclei have been used in the compilation.

Fig. 10 - The photoneutron cross section for ^{160}Gd, from Berman and Fultz (1975).

Fig. 11 - The giant quadrupole vibration in ^{90}Zr, excited by 152 MeV α-particle scattering (Bertrand, et al., 1980).

Fig. 12 - Quadrupole strength function in ^{24}Mg, inferred from inelastic α-particle scattering (Bertrand, et al., 1978). The integrated strength function for the observed discrete states is plotted as the staircase solid line. The dashed curve shows the integrated strength of a Breit-Wigner distribution, assuming a width of 8 MeV.

Fig. 13 - Systematics of the width of the giant quadrupole vibration, from Bertrand (1981).

Fig. 14 - The extracted angular distribution of the giant vibrational peak in α scattering from ^{144}Sm, separated into two components (Youngblood, et al., 1977). The upper component is enhanced at the smallest scattering angles, showing its monopole character.

Figure Captions (continued)

Fig. 15 - The energy spectrum in the (p,n) reaction at 200 MeV and 0° scattering angle (Gaarde, et al., 1981). The Gamow-Teller giant vibration is prominent in all closed shell nuclei having a neutron excess.

Fig. 16 - The theoretical quadrupole strength function in ^{209}Pb, from Broglia and Winther (1981). The upper histogram shows the response in the independent particle model, and the lower histogram shows the RPA response. Note that a low state emerges with considerable strength, and the strength at higher excitation becomes more concentrated.

Fig. 17 - The RPA octupole response in ^{208}Pb, calculated by Ring and Speth (1974). The states below 5 MeV excitation have negligible strength in the independent particle model, but in RPA the lowest state acquires a major fraction of the total strength.

Fig. 18 - The dipole response function in ^{208}Pb, calculated by Shlomo and Bertsch (1975). The widths of individual peaks are actual escape widths in the RPA theory. The escape width is seen to be small compared to the total width.

Figure Captions (continued)

Fig. 19 - The imaginary optical potential depth. The thin lines are the infinite nuclear matter calculations of Jeukenne, Lejeune, and Mahaux (1976). The lower and upper curves are for nuclear matter density and $\rho_0/2$ nuclear matter density, respectively. We have extrapolated the published curves to zero energy using the parameterization of eq. (33). The heavy solid lines are the empirical potential depths for the surface and volume parts of the absorptive potential from Rapaport, et al., (1979), quoted in eq. (5).

Fig. 20 - Perturbation graphs for the imaginary self-energy of particles.

Fig. 21 - The single-particle damping width $\Gamma(E)$ as a function of energy, for the $s_{1/2}$ state in ^{208}Pb (Bertsch, et al., 1979). The solid lines is the theory eq. (B9) with $\Delta = 0.5$ MeV. Dots and squares are empirical values based on eq. (28) and various optical potentials.

Fig. 22 - Perturbation graphs for the damping of a vibration. On the top is shown the coherent sum of amplitudes for doorway coupling via the particle and the hole. They give rise to the four contributions to the imaginary part of the self-energy of the vibration. The two graphs on the left arise from the independent damping of the particle and the hole, and the two remaining graphs give an interference.

Figure Captions (continued)

Fig. 23 - The perturbation graph for the coupling between a vibrational state and double vibration, used in the vibrational damping model of Soloviev, et al. (1977).

Fig. 24 - Giant dipole strength function in ^{120}Sn, calculated by Soloviev, et al. (1977), including damping into two-phonon doorways. An averaging interval of 0.1 MeV was used in plotting the results.

Fig. 25 - Histogram of the square of the sum of the particle and hole contributions to the matrix elements coupling the p-h+v states to the giant quadrupole vibration in ^{208}Pb. Dashed histogram shows the independent contributions of particle and hole matrix elements, and the solid histogram is the coherent sum.

Fig. 26 - Self-energy graphs for vibrational damping with particle-hole-vibration doorways.

Fig. 27 - Perturbation theory graphs associated with the collision integral (C7). The graphs represent contributions to $\delta n(p)$, coming from different terms in the expansion of (C7) to first order in $\delta n(p)$, $\delta n(p')$.

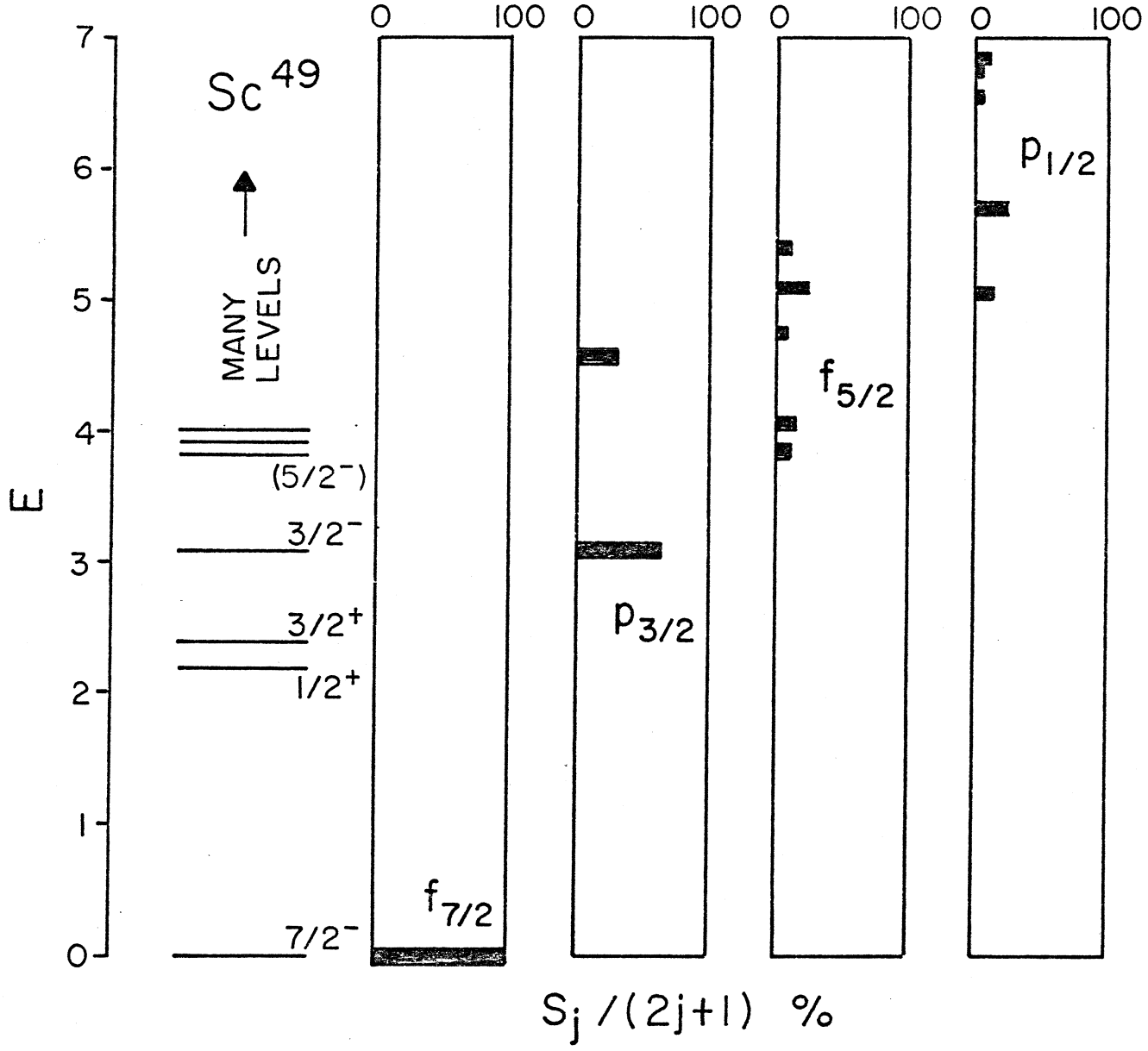
Sc 49
MANY LEVELS
(5/2⁻)
3/2⁻
3/2⁺
1/2⁺
7/2⁻
E
0
1
2
3
4
5
6
7
0
100
f7/2
p3/2
f5/2
p1/2
Sj /(2j+1) %

FIGURE 1

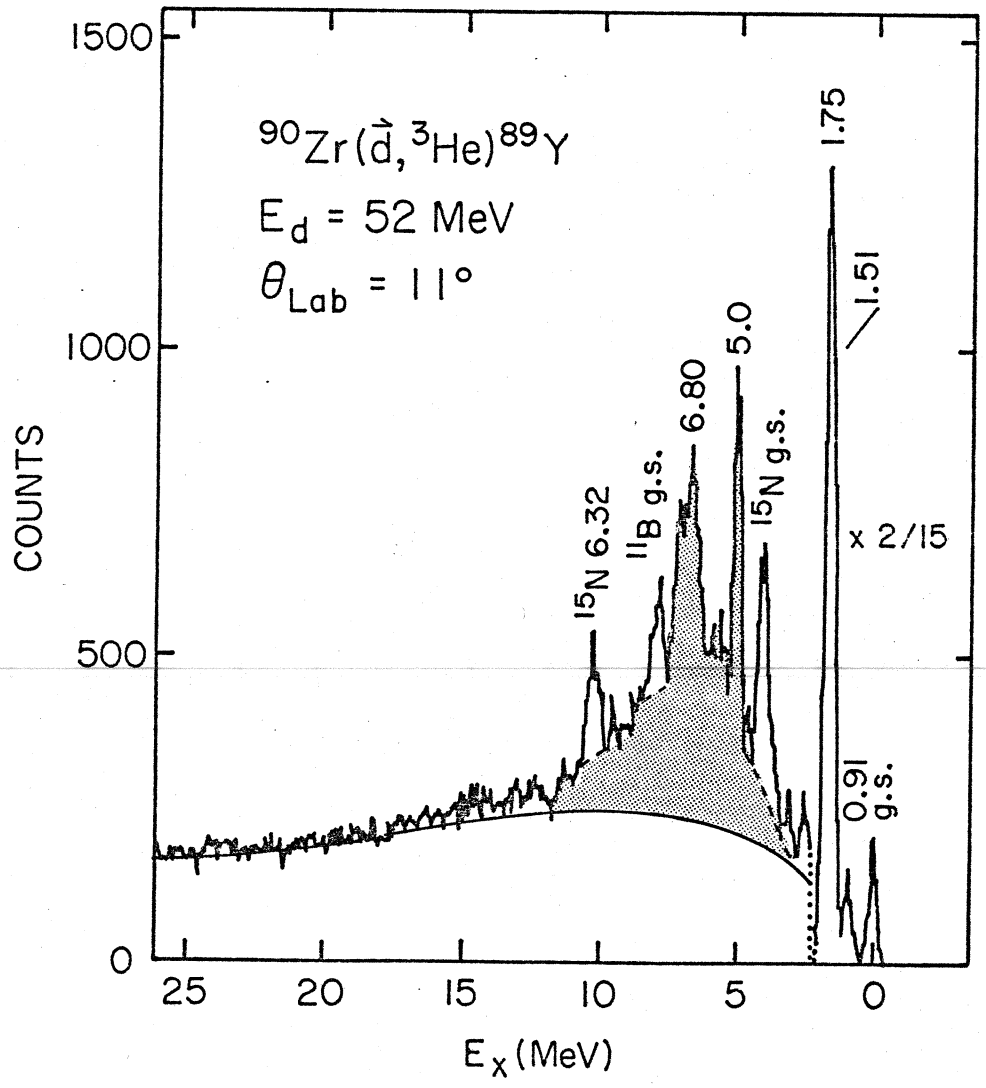
1500
1000
500
0
COUNTS
$^{90}Zr(\vec{d},{}^{3}He)^{89}Y$
E_d = 52 MeV
θ_{Lab} = 11°
^{15}N 6.32
^{11}B g.s.
6.80
5.0
^{15}N g.s.
1.75
1.51
x 2/15
0.91
g.s.
25
20
15
10
5
0
E_x (MeV)

FIGURE 2

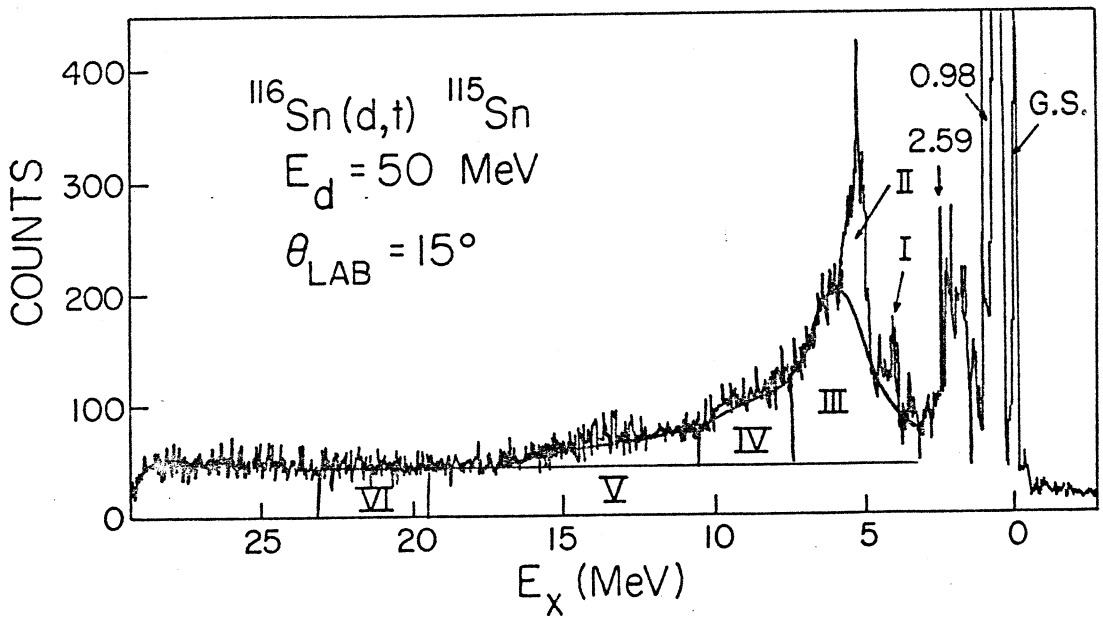
^{116}Sn (d,t) ^{115}Sn
E_d = 50 MeV
θ_{LAB} = 15°
COUNTS
400
300
200
100
0
25
20
15
10
5
0
E_x (MeV)
0.98
G.S.
2.59
I
II
III
IV
V
VI

FIGURE 3

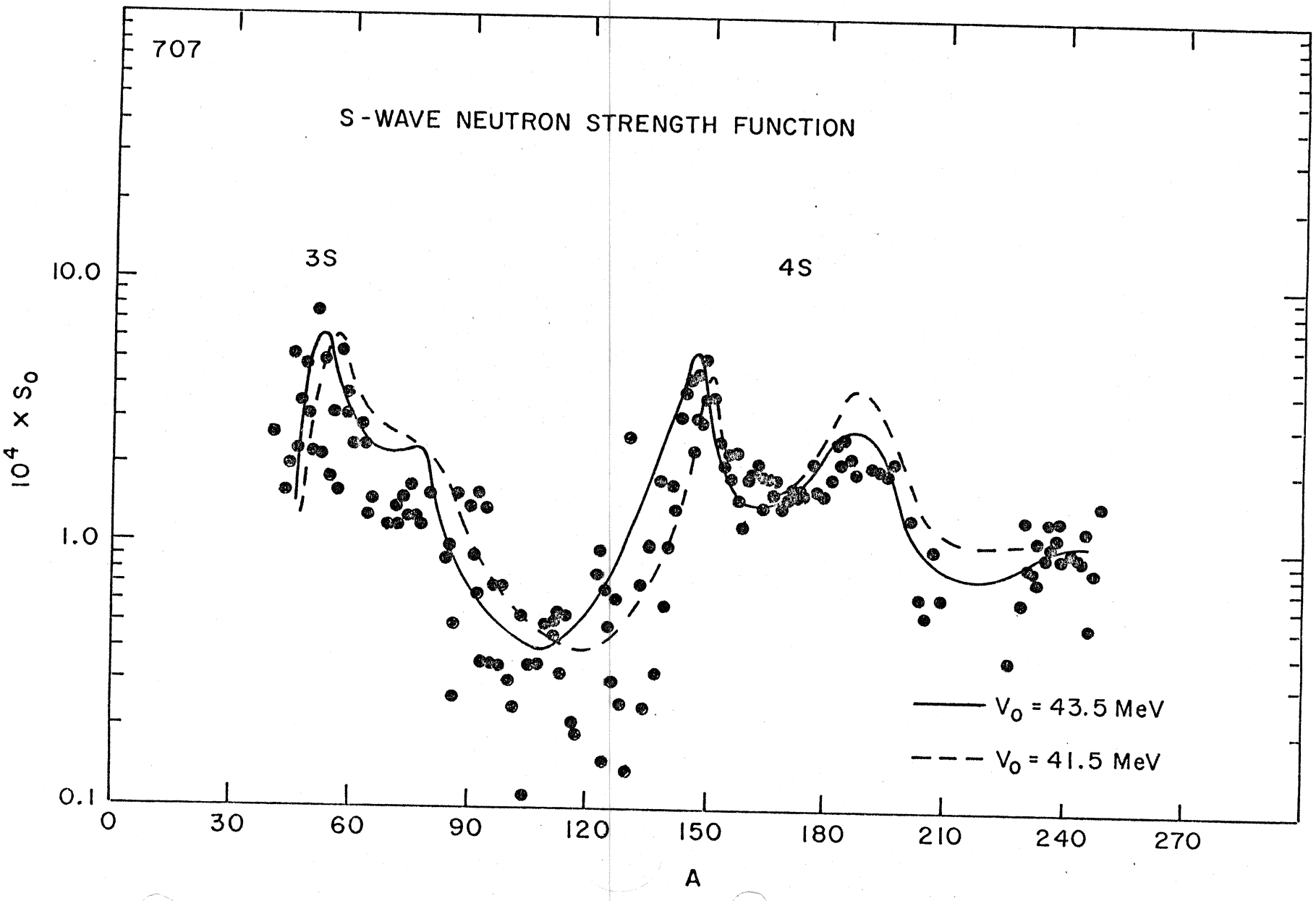
707
S-WAVE NEUTRON STRENGTH FUNCTION
3S
4S
10.0
1.0
0.1
$10^4 \times S_0$
0
30
60
90
120
150
180
210
240
270
A
V_0 = 43.5 MeV
V_0 = 41.5 MeV

FIGURE 4

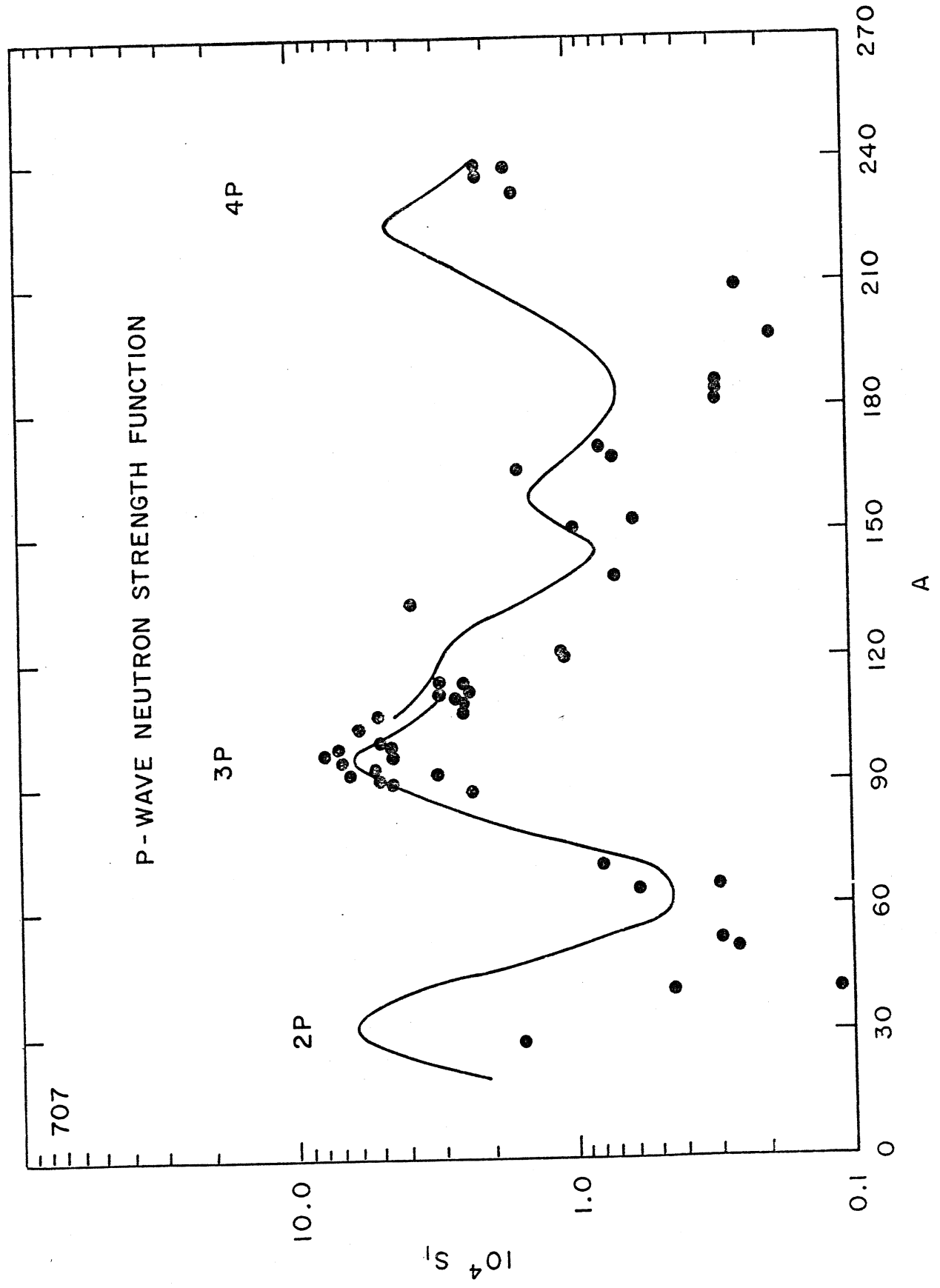
P-WAVE NEUTRON STRENGTH FUNCTION
707
2P
3P
4P
10^4 S_1
10.0
1.0
0.1
0
30
60
90
120
150
180
210
240
270
A

FIGURE 5

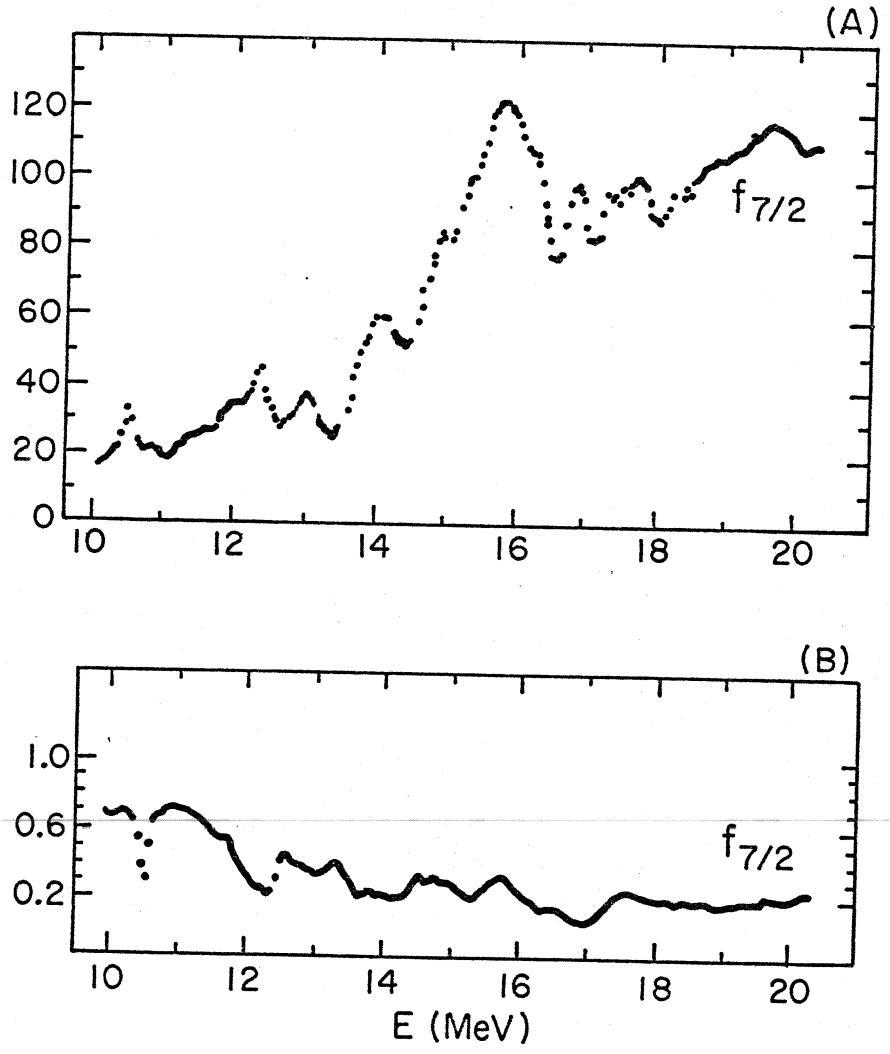
(A)
120
100
80
60
40
20
0
10
12
14
16
18
20
$f_{7/2}$
(B)
1.0
0.6
0.2
10
12
14
16
18
20
E (MeV)
$f_{7/2}$

FIGURE 6

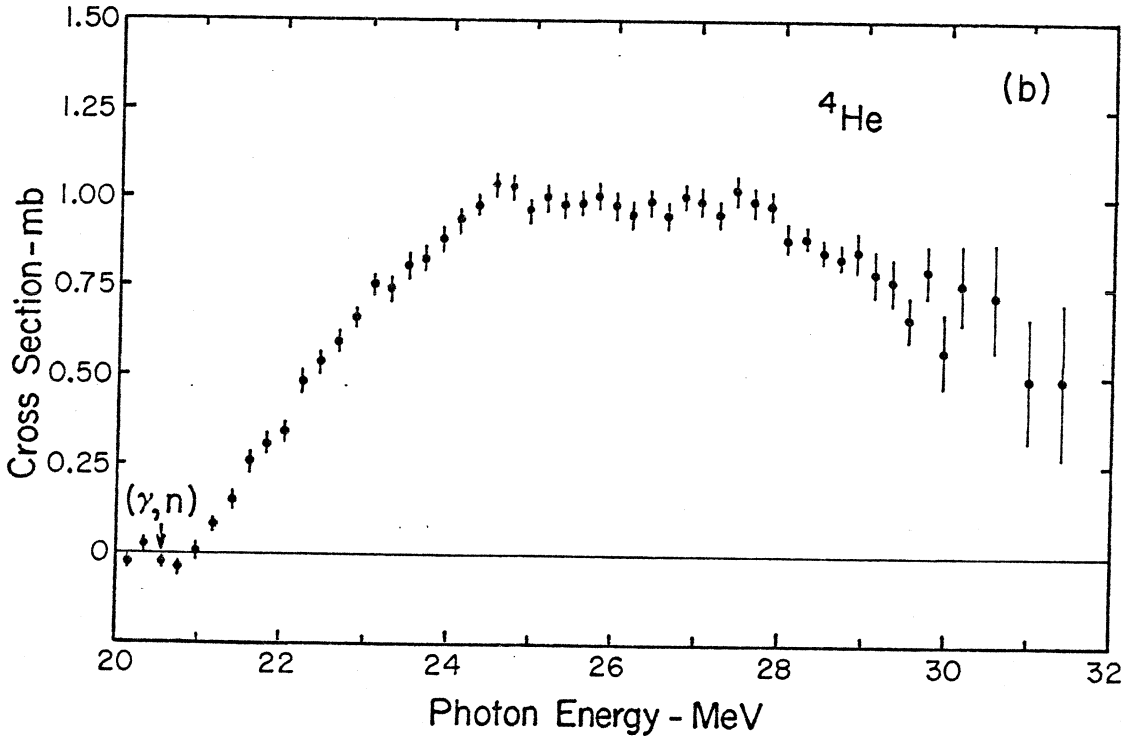
1.50
1.25
1.00
0.75
0.50
0.25
0
Cross Section - mb
(γ,n)
^{4}He
(b)
20
22
24
26
28
30
32
Photon Energy - MeV

FIGURE 7

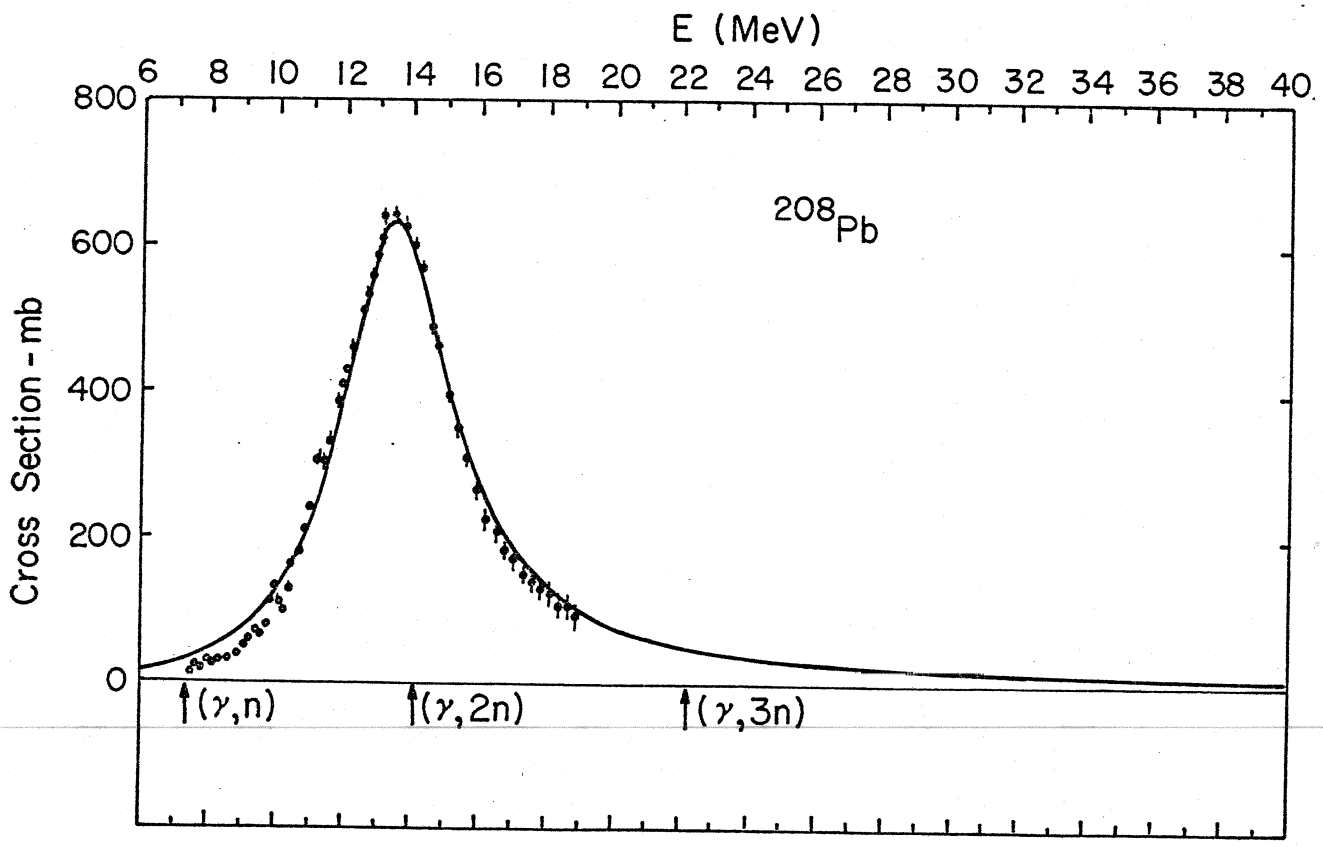
E (MeV)
6 8 10 12 14 16 18 20 22 24 26 28 30 32 34 36 38 40
800
600
400
200
0
Cross Section - mb
208Pb
(γ,n)
(γ,2n)
(γ,3n)

FIGURE 8

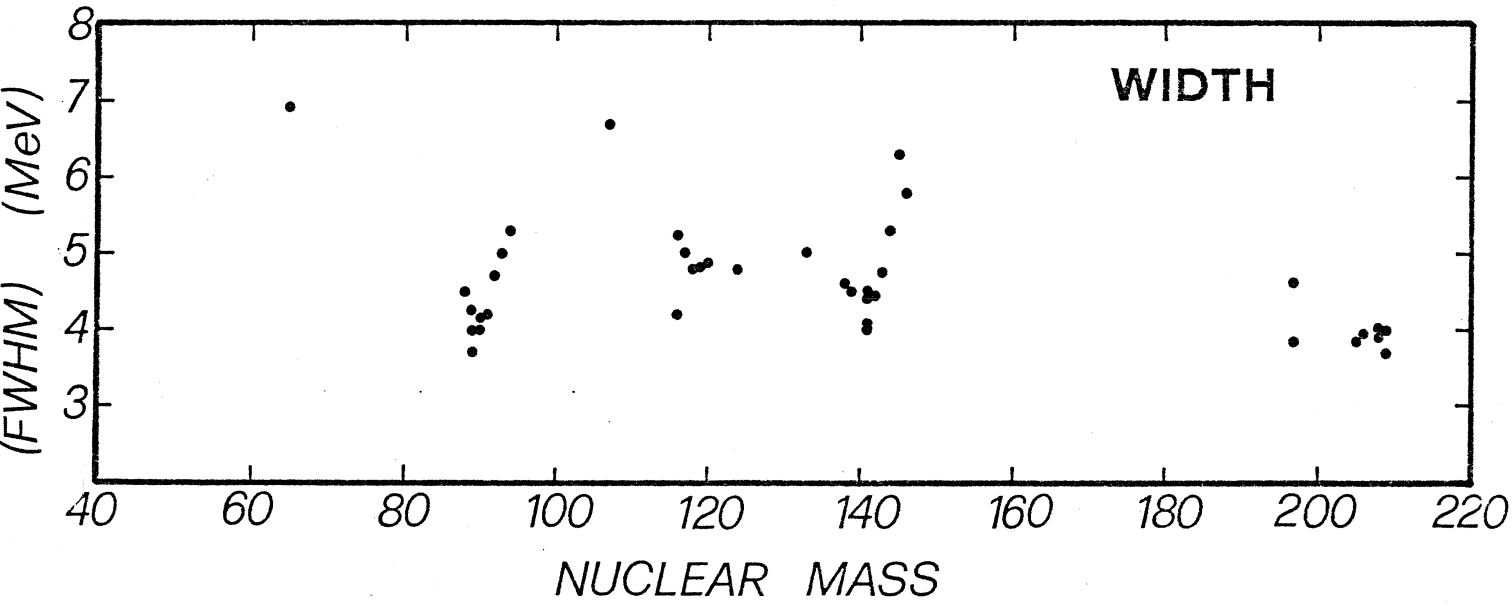
WIDTH
(FWHM) (MeV)
8
7
6
5
4
3
40
60
80
100
120
140
160
180
200
220
NUCLEAR MASS

FIGURE 9

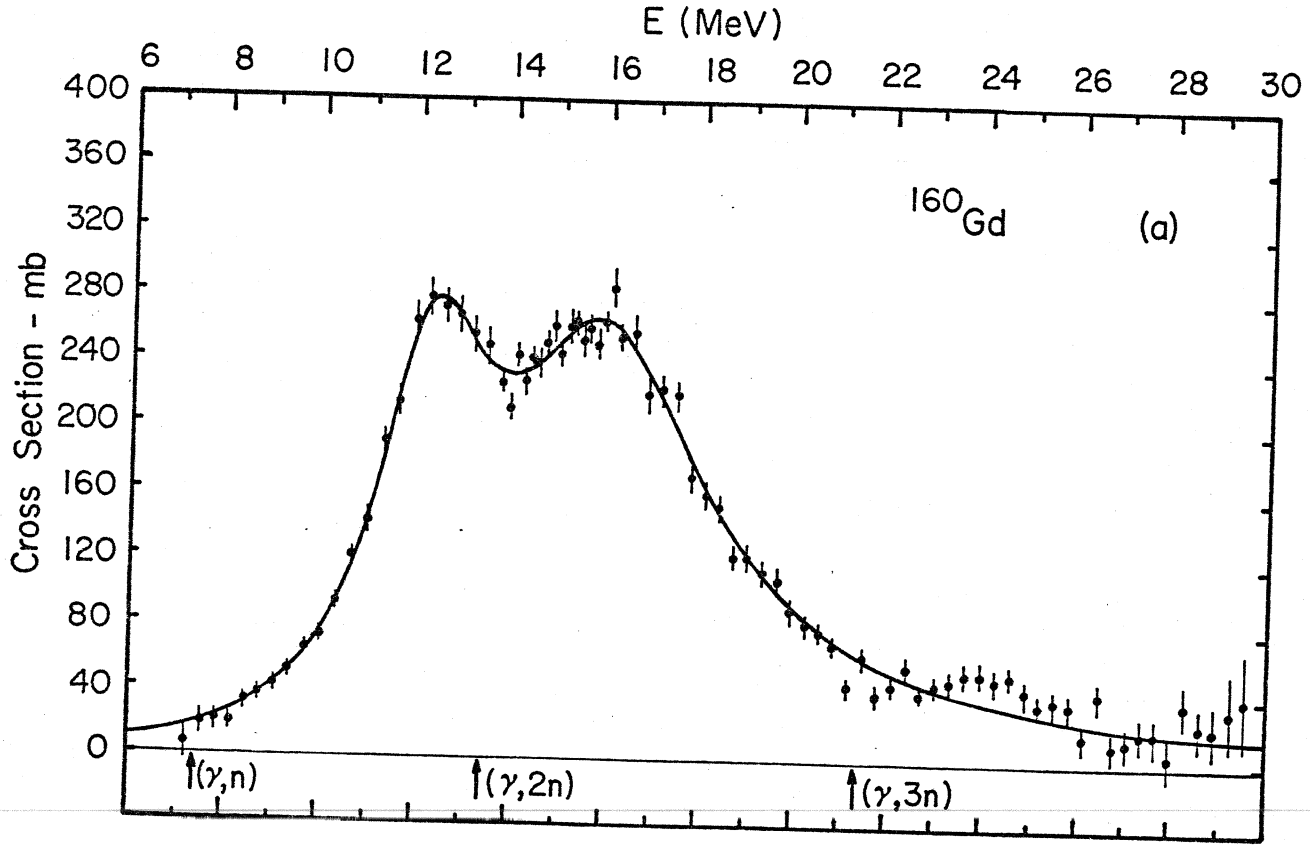
E (MeV)
6
8
10
12
14
16
18
20
22
24
26
28
30
400
360
320
280
240
200
160
120
80
40
0
Cross Section - mb
160Gd
(a)
(γ,n)
(γ,2n)
(γ,3n)

FIGURE 10

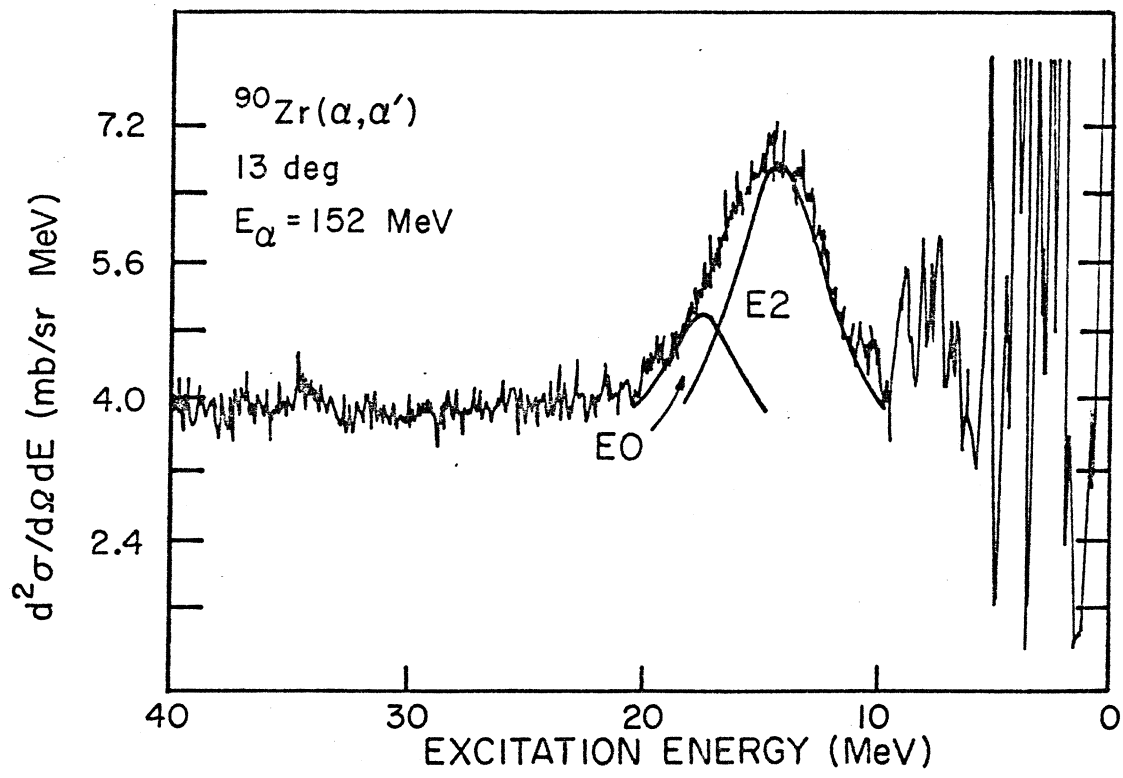
$^{90}Zr(\alpha,\alpha')$
13 deg
E_α = 152 MeV
E2
E0
7.2
5.6
4.0
2.4
$d^2\sigma/d\Omega dE$ (mb/sr MeV)
40
30
20
10
0
EXCITATION ENERGY (MeV)

FIGURE 11

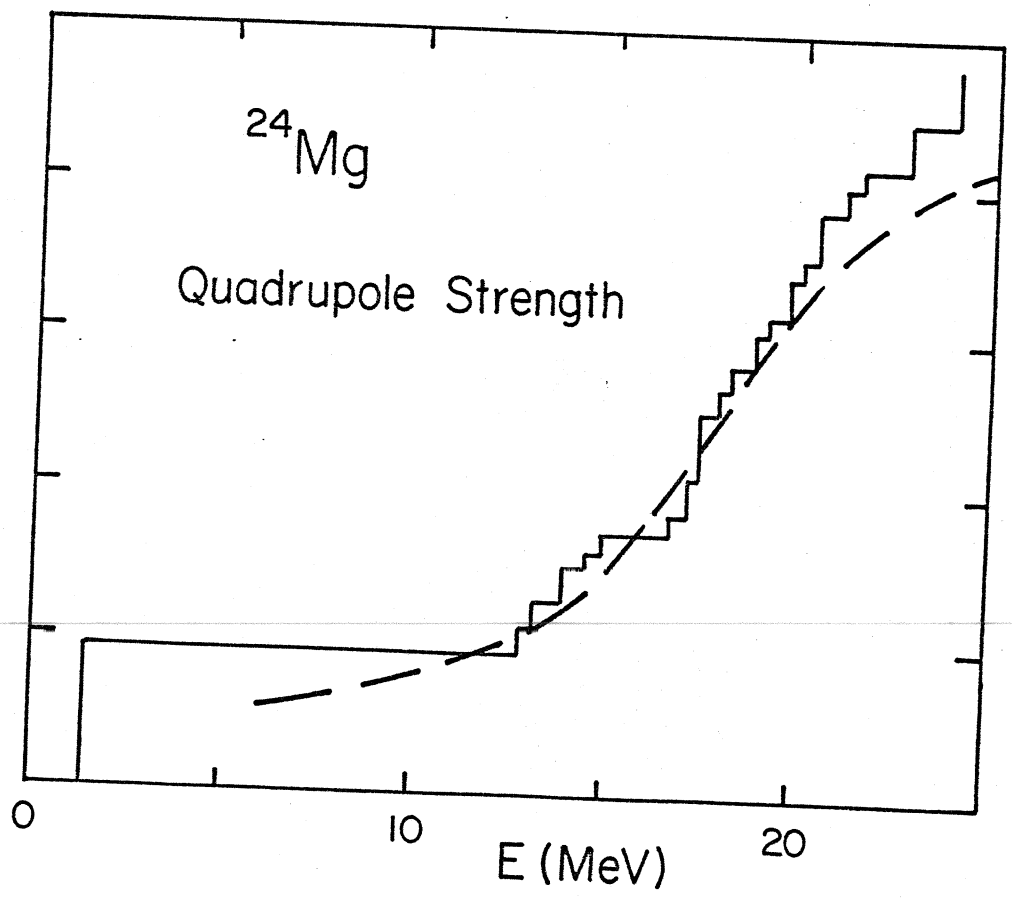

FIGURE 12

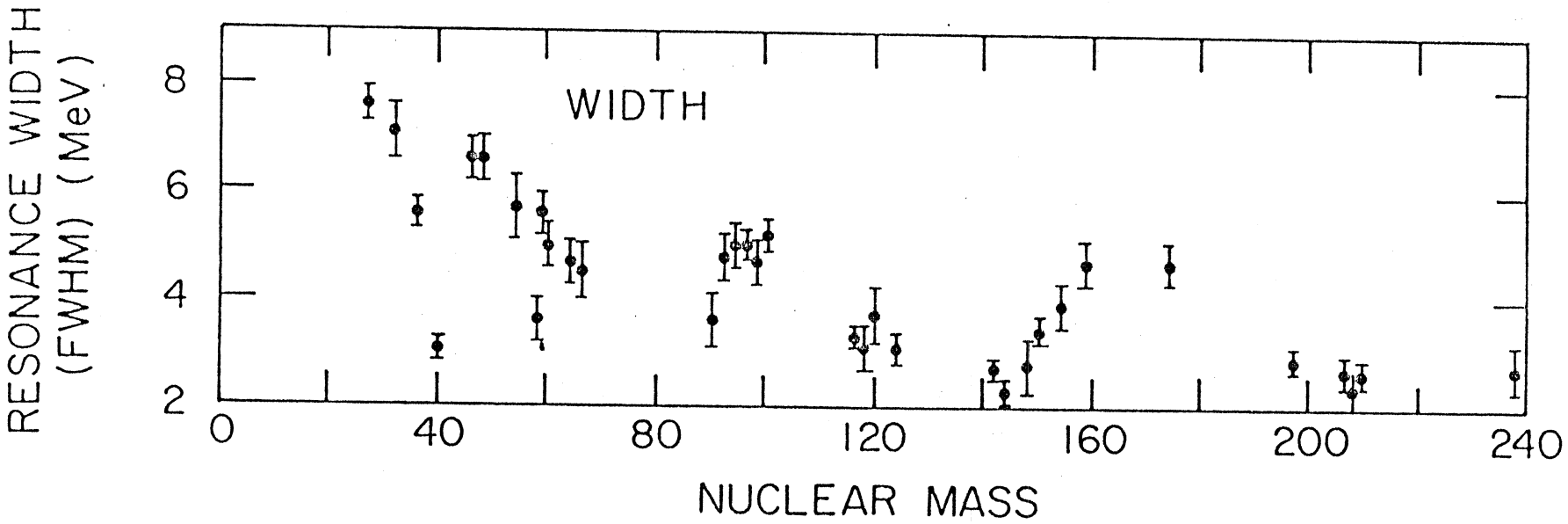
RESONANCE WIDTH
(FWHM) (MeV)
WIDTH
8
6
4
2
0
40
80
120
160
200
240
NUCLEAR MASS

FIGURE 13

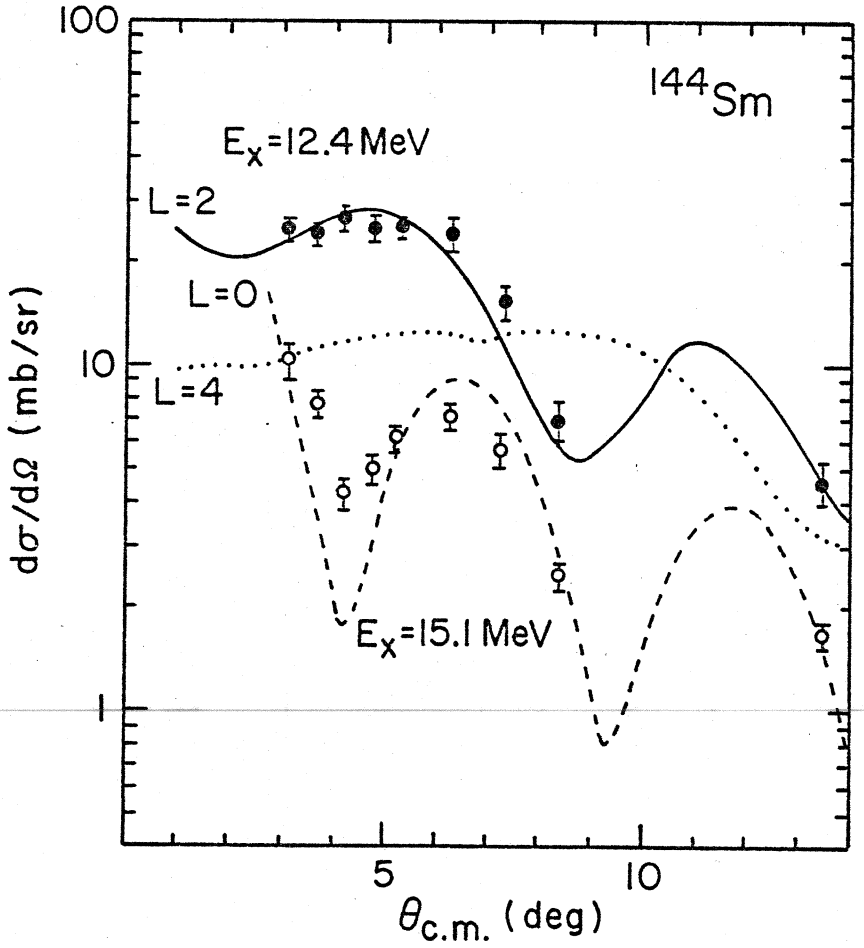
100
10
1
^{144}Sm
E_x=12.4 MeV
L=2
L=0
L=4
E_x=15.1 MeV
$d\sigma/d\Omega$ (mb/sr)
5
10
$\theta_{c.m.}$ (deg)

FIGURE 14

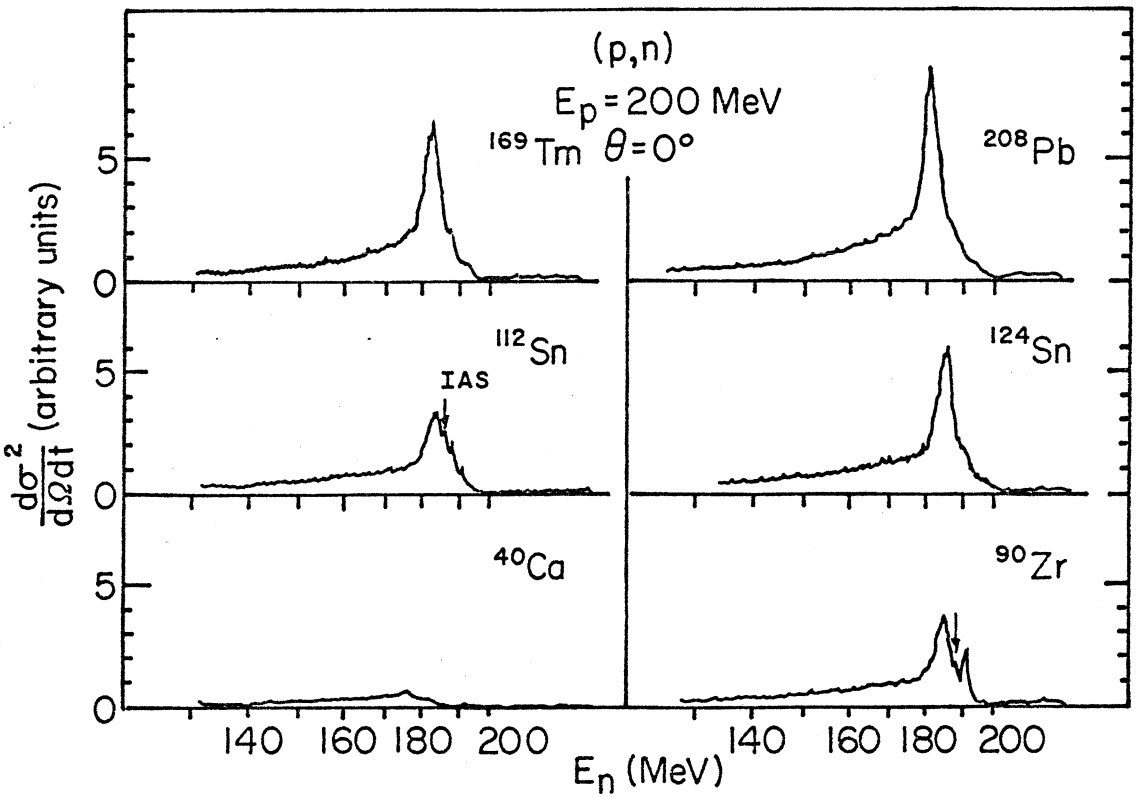
(p,n)
Ep = 200 MeV
169Tm θ=0°
208Pb
112Sn
IAS
124Sn
40Ca
90Zr
dσ²/dΩdt (arbitrary units)
5
0
140 160 180 200
En (MeV)

FIGURE 15

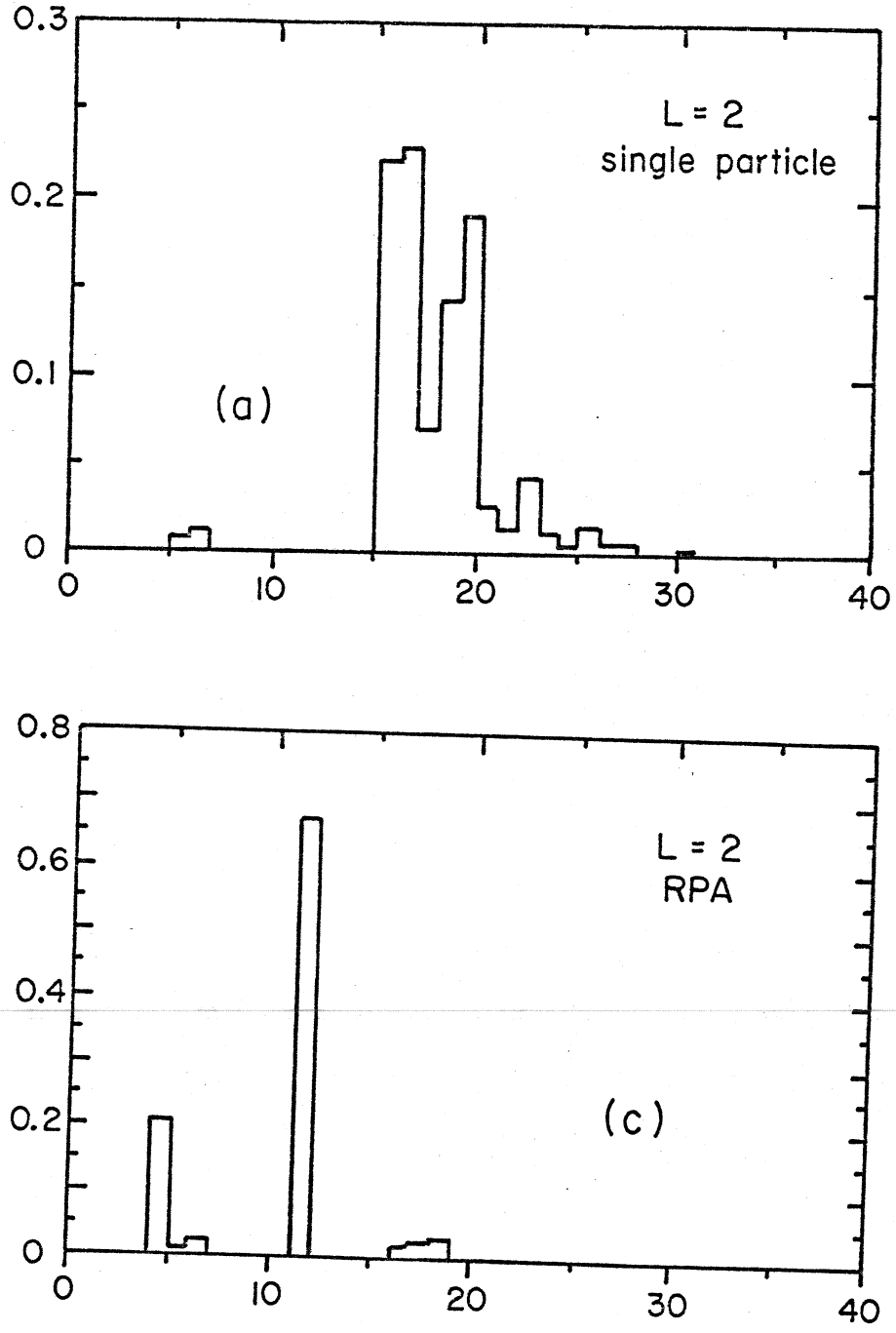
0.3
0.2
0.1
0
0
10
20
30
40
L = 2
single particle
(a)
0.8
0.6
0.4
0.2
0
0
10
20
30
40
L = 2
RPA
(c)

FIGURE 16

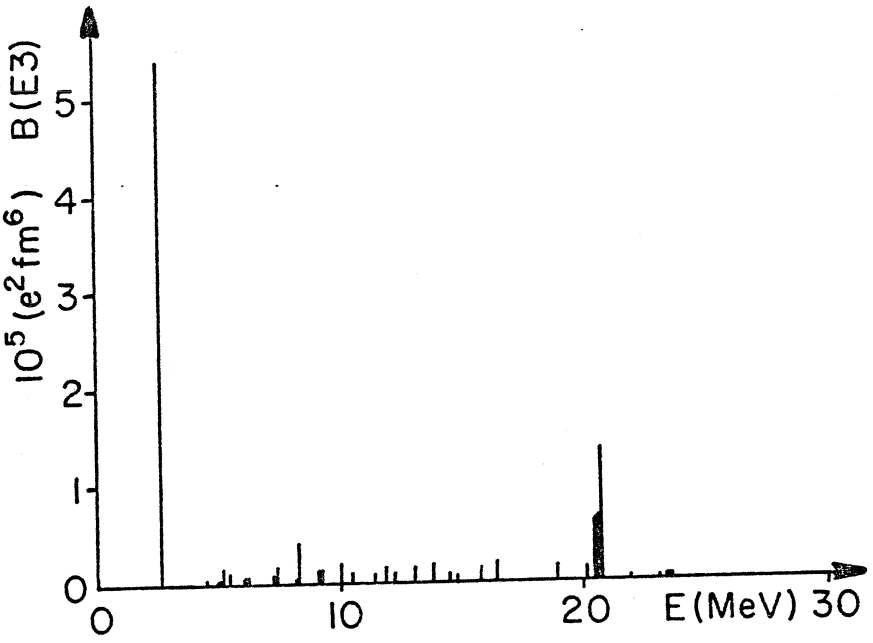

FIGURE 17

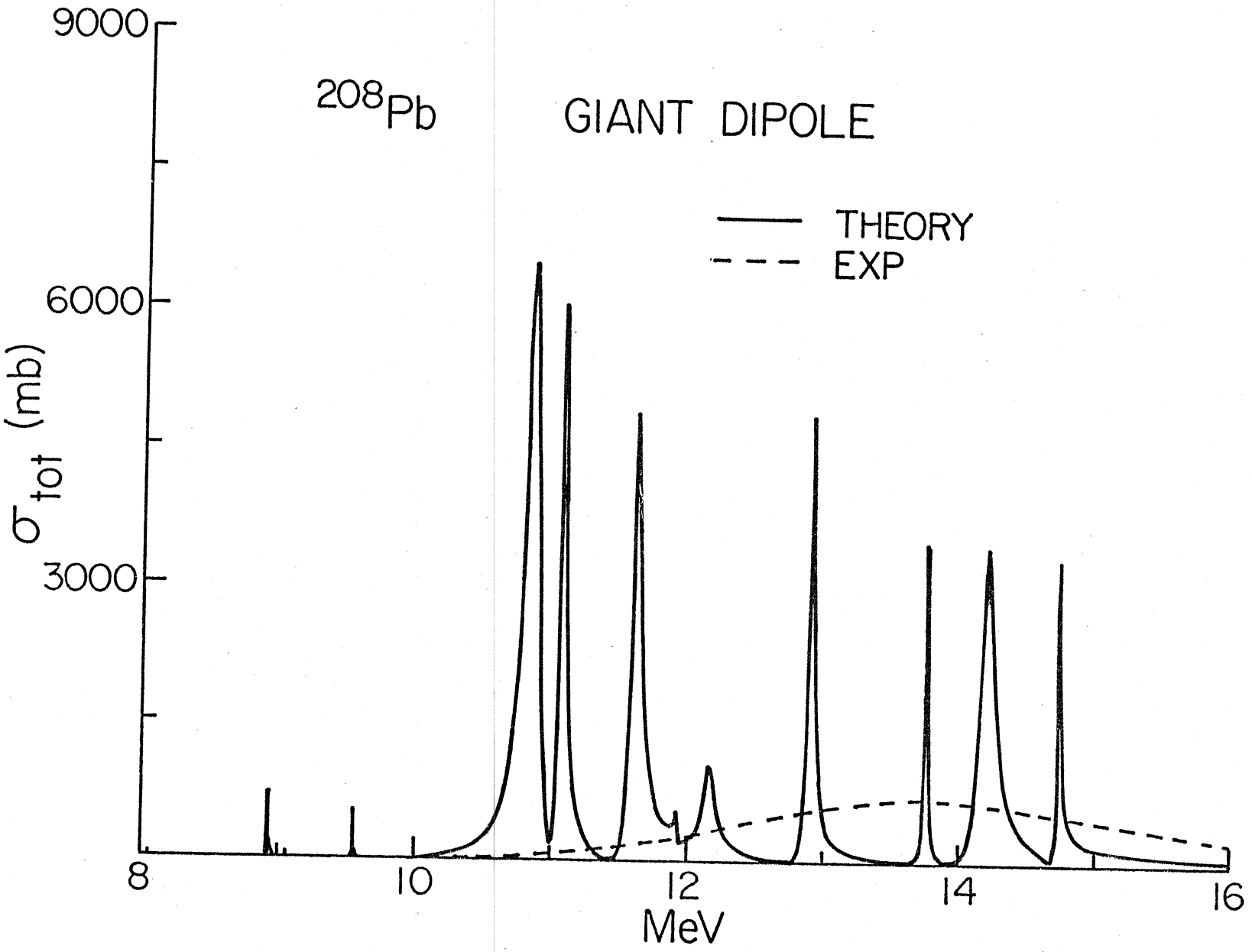
9000
6000
3000
σ_{tot} (mb)
^{208}Pb
GIANT DIPOLE
THEORY
EXP
8
10
12
14
16
MeV

FIGURE 18

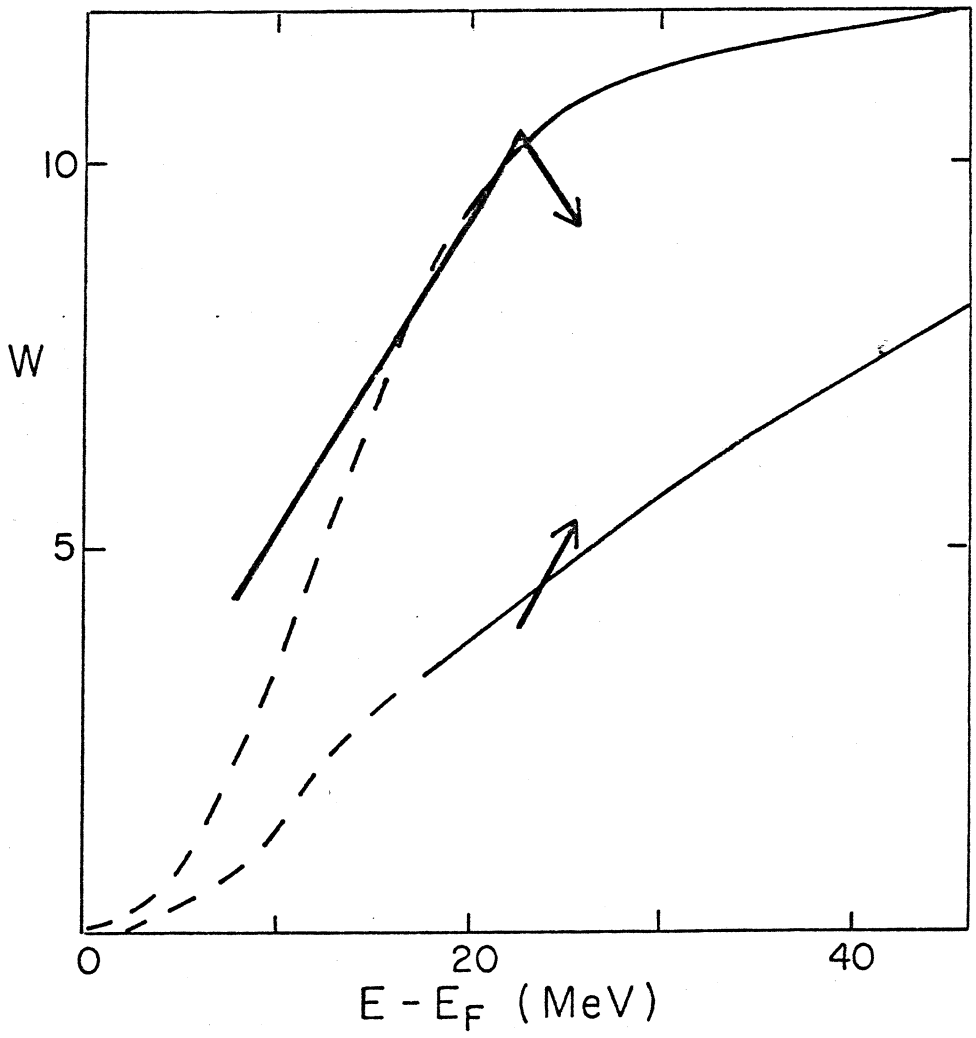

FIGURE 19

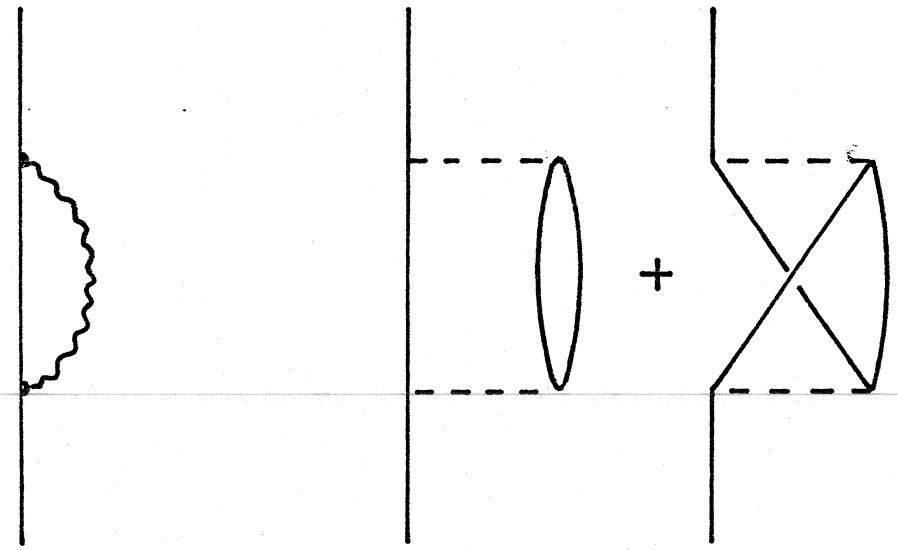

FIGURE 20

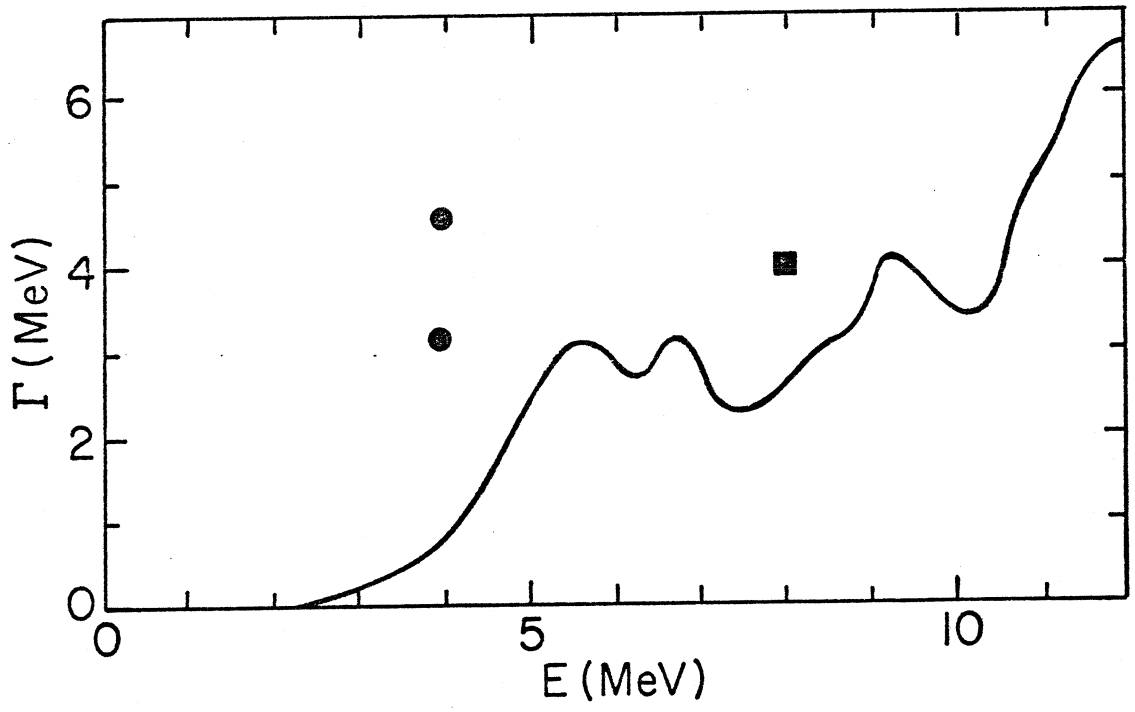

FIGURE 21

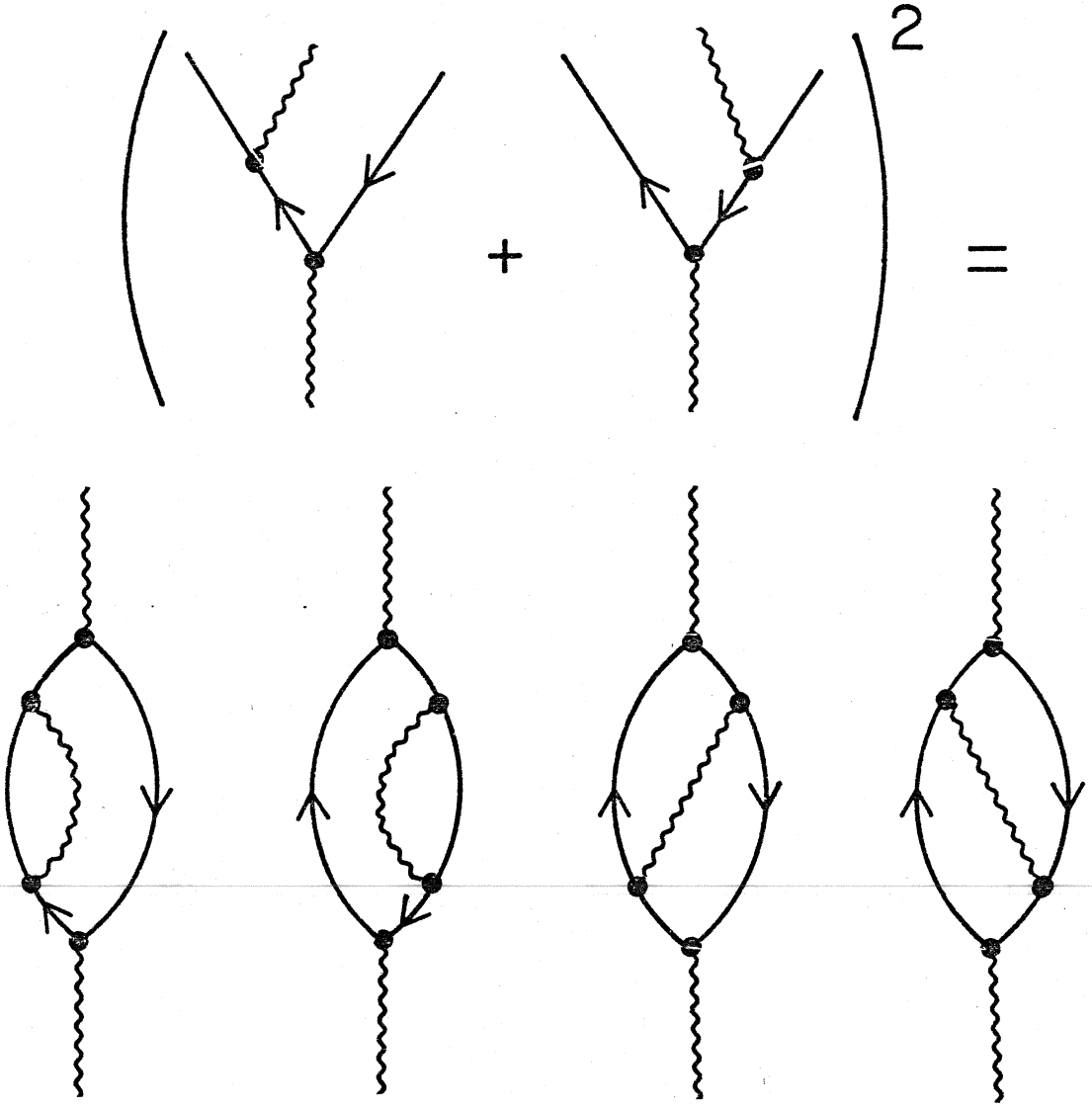

FIGURE 22

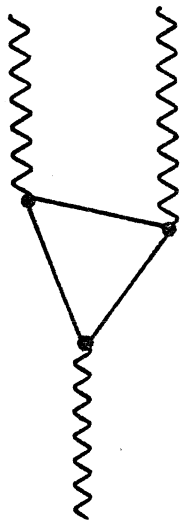

FIGURE 23

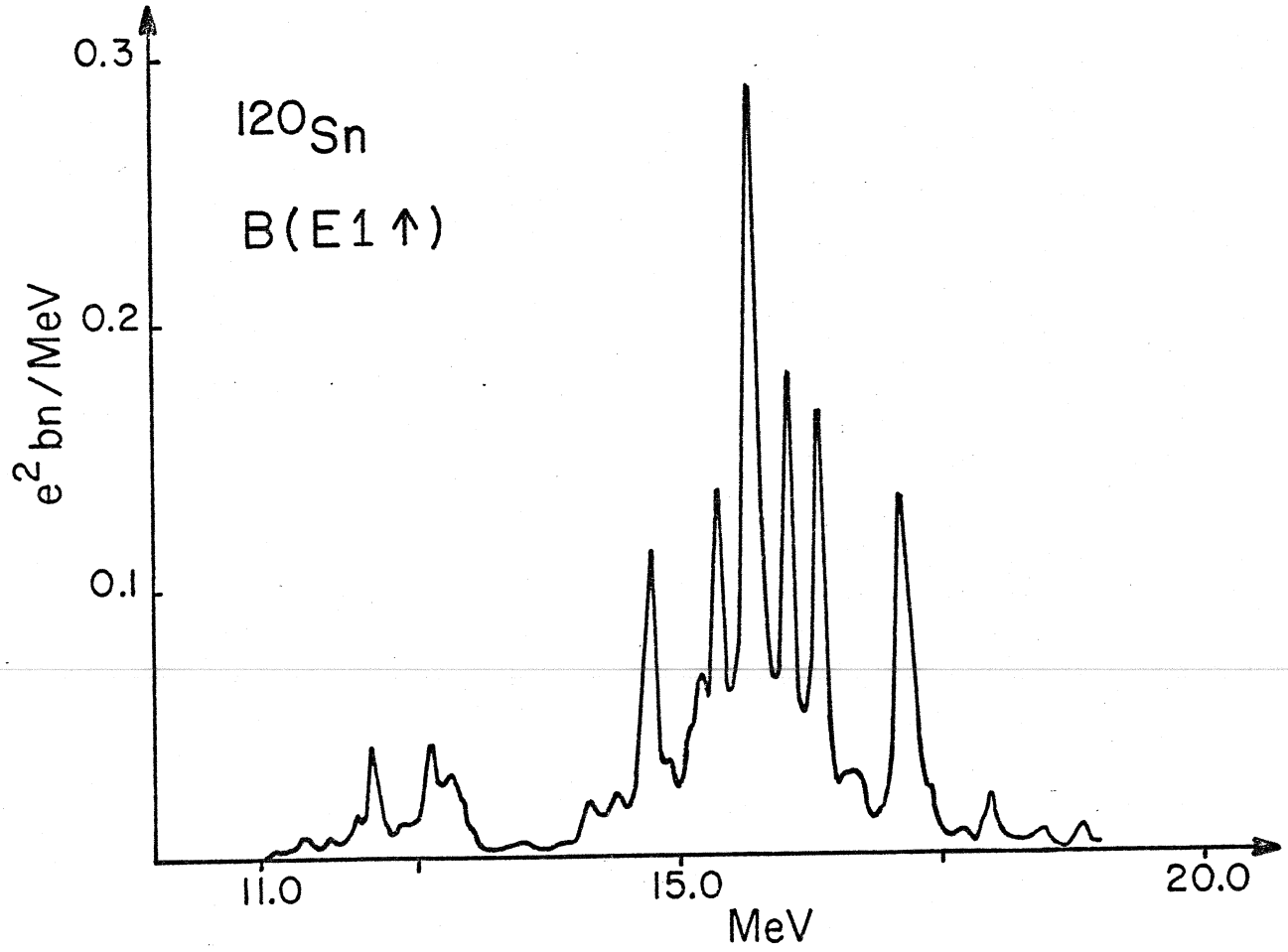

FIGURE 24

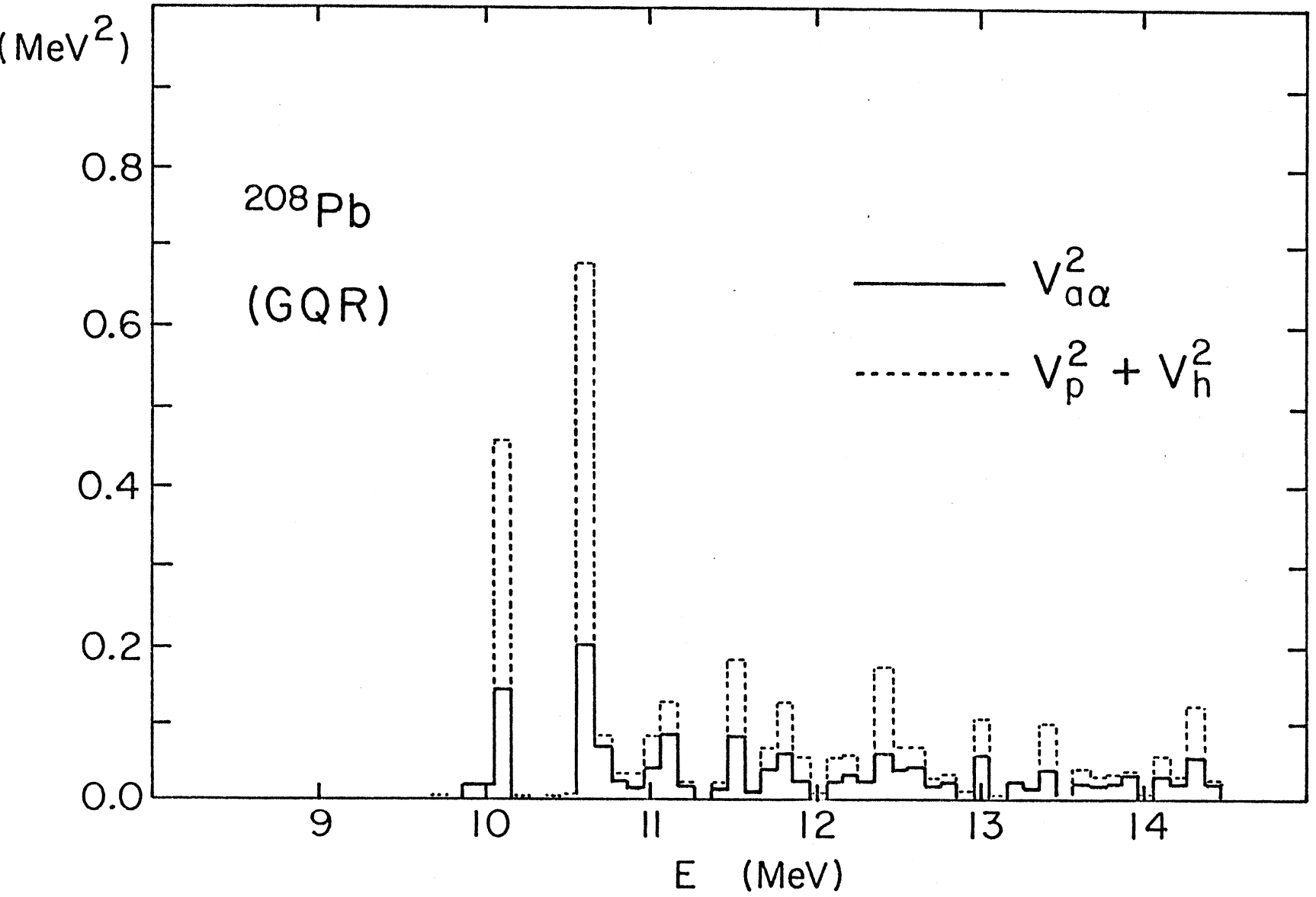
(MeV^2)
0.8
0.6
0.4
0.2
0.0
^{208}Pb
(GQR)
$V^2_{a\alpha}$
$V^2_p + V^2_h$
9
10
11
12
13
14
E (MeV)

FIGURE 25

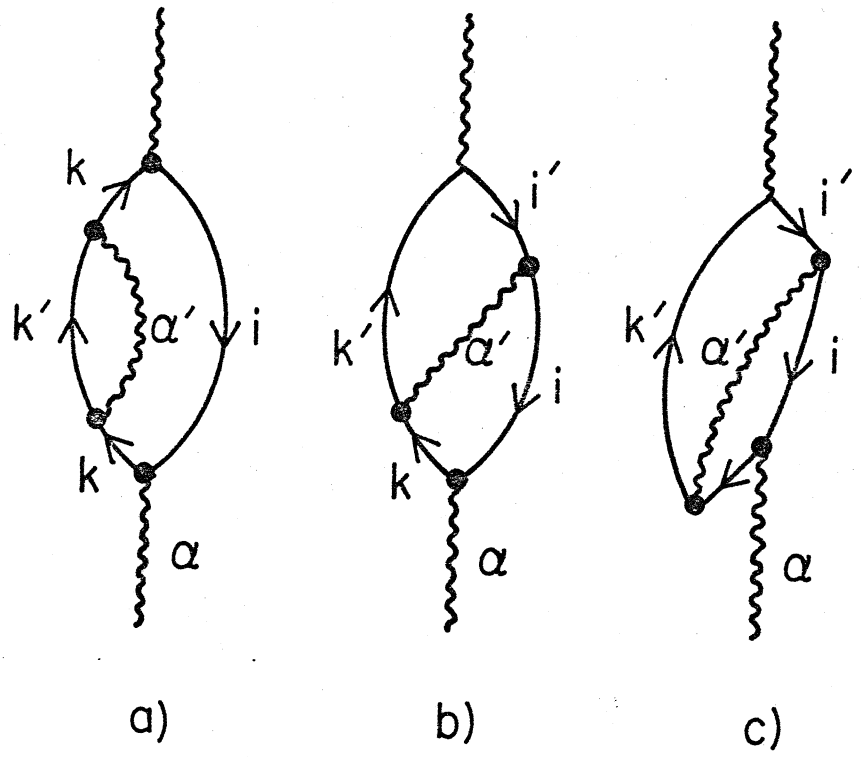

FIGURE 26

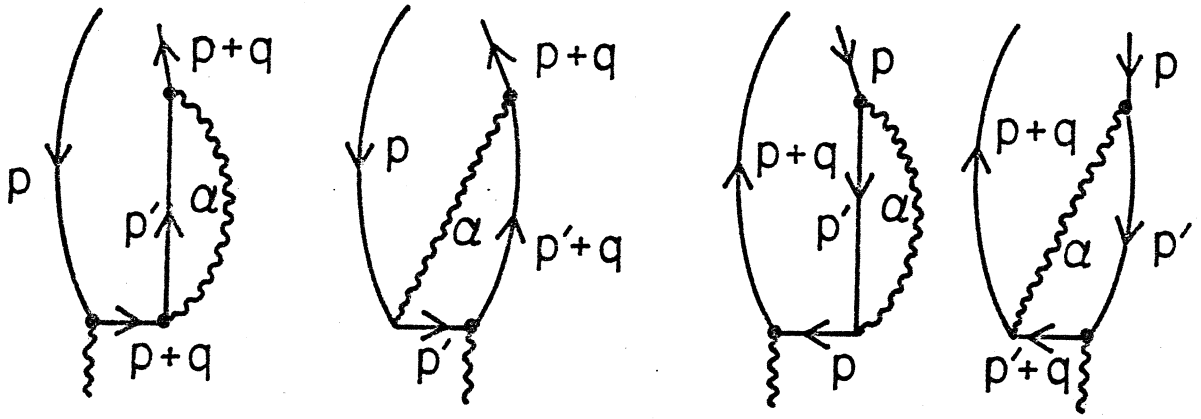

FIGURE 27